Analysis of different hypotheses for modeling air–water exchange and temperature evolution in a tropical reservoir

Juliana-Andrea Alzate-Gómez, Hélène Roux, Ludovic Cassan, Thomas Bonometti, Jorge Alberto Escobar Vargas, Luis-Javier Montoya Jaramillo

Journal of
Water & Climate Change

IWA PUBLISHING

Journal of Water and Climate Change Vol 15 No 2, 773 doi: 10.2166/wcc.2023.567

Analysis of different hypotheses for modeling air–water exchange and temperature evolution in a tropical reservoir

Juliana-Andrea Alzate-Gómez [a,b,*], Hélène Roux [b], Ludovic Cassan [b], Thomas Bonometti[b], Jorge Alberto Escobar Vargas[c] and Luis-Javier Montoya Jaramillo [d]

[a] Faculty of Basic Science, University of Medellin, Medellin, Colombia
[b] Institut de Mécanique des Fluides de Toulouse (IMFT), Toulouse, France
[c] Faculty of Civil Engineering, Pontifical Javierian University, Bogota, Colombia
[d] Faculty of Engineering, University of Medellin, Medellin, Colombia
*Corresponding author. E-mail: jalzate321@soyudemedellin.edu.co

J-AA, 0000-0002-9029-6989; HR, 0000-0001-7076-5015; LC, 0000-0002-2493-0646; L-JM, 0000-0002-5832-2219

ABSTRACT

The present analysis shows that the most crucial parameter for a correct representation of the observed temperature behavior are the heat exchange coefficient and the wind. The different approaches tested all have limitations, but they can reproduce reservoir temperature trends at different depths with a maximum standard deviation ranging from 3 °C to 8 °C.

Key words: 3D numerical model, heat exchange, thermal processes, tropical reservoir, water quality

HIGHLIGHTS

- Tropical reservoir's water temperature is strongly influenced by air–water heat exchanges, but the fast exchanges of temperature in tropical zones made traditional formulations of exchange coefficients to be insufficient.
- The parameter that mainly affects the heat transfer and thermal stratification process is the transfer coefficient A and can be used as an approximation for estimating the exchange rate of the reservoir.

1. INTRODUCTION

The construction, operation, and removal of large reservoirs are fundamental environmental issues because of the benefits they generate and the environmental impact they have. Hydroelectricity production accounts for 16% of total energy production (Killingtveit 2019) but, in the American continent, it is the largest source of energy production. In addition, they have essential functions such as supplying water to cities, irrigation, and energy. While these dams have brought some benefits, they have also brought severe and irreversible changes to the natural hydrology of the river, affecting soil, vegetation, biodiversity, landscape, atmosphere, and, in turn, watersheds (Agostinho *et al.* 2008; Kuriqi *et al.* 2021), reducing water flow, increasing water residence time, thermal stratification, increasing sedimentation rates and decreasing dissolved oxygen concentrations, among others (Pimenta *et al.* 2012).

The impact on reservoir water quality is a significant concern in ecological management. Life quality is highly constrained by water quality, which is affected by the quality of reservoirs built for hydroelectric projects and water supply. Building dams is particularly important for many Latin-American countries, where most of the electric supply comes from hydropower and many reservoirs. Thermal stratification caused by solar heating plays a significant role in determining water quality in the reservoir. In tropical countries, lakes and impoundments will stratify during the year as a result of increasing temperature differences between the warm upper (epilimnion) and cold lower (hypolimnion) layers of water (Halini Baharim *et al.* 2011). Air temperatures can vary by up to 10 °C from day to day, with water temperatures ranging from 20 to 32 °C.

Temperature studies in reservoirs have ranged from field measurements to computer tools, such as modeling. In the case of tropical reservoirs, from a data analysis and statistical point of view, research focuses on (1) describing and characterizing thermal distribution by field observations, such as the characterization of the stratification pattern and affectation of these thermal regimes in response to climate variables; (2) reservoir biochemistry and aquatic biology and the relations between them.

In Labaj *et al.* (2018), a data logger recorded temperature profiles hourly and measured every 2 m at a point at a maximum depth of 30 m in four lakes in Ecuador. They observed that thermal stratification was significantly positively correlated with air temperature and negatively correlated with wind speed across all lakes, and the most critical finding was that the high-resolution data showed that stratification did not breakdown overnight. In Lewis (1996), a theoretical comparison of the characteristics of several tropical and temperate lakes was carried out. The main finding of this study was that the comparison of tropical and temperate lakes has excellent potential to demonstrate lake function in general and is typified by non-seasonal substantial variations superimposed on seasonal cycles in most cases. Elçi (2008) studied the effects of thermal stratification and mixing on reservoir water quality at one point in the reservoir over 14 days using a water quality meter. Multivariate analysis was carried out on a data matrix of seven variables. The results showed that air temperature, lagged wind speed, and humidity influence variations in water quality parameters. In Rangel *et al.* (2009), temperatures are measured with a portable digital meter, in two main climatological seasons: cool-dry season and warm-rainy season, at a central reservoir point, at the surface, 1.5, 2.5, and 4 m. The main finding of this study was that the thermal pattern strongly influenced the vertical distribution of the phytoplankton community. Pajares *et al.* (2017) observed that temperature and oxygen stratification shaped the distribution of picoplankton. In Huszar *et al.* (2006), the data set includes 192 aquatic systems sampled on seasonal bases for at least 1 year using average values. They found significant differences in nutrient–chlorophyll ratios and thermal profiles between tropical and temperate climates. Amorim *et al.* (2020) monitor ten reservoirs in Brazil to study cyanobacterial blooms. They demonstrated that omnivorous crustaceans and total dissolved phosphorus mainly influenced cyanobacterial biomass. Solar radiation, air temperature, mixing zone, and salinity also significantly explain biomass behavior. These studies highlight the importance of thermal stratification as one of the main factors affecting variation within the water column of tropical lakes. However, in evaluating the thermal structure of the reservoir through data analysis, it is difficult to measure and verify the quality of the data, and it is difficult to propose an analysis and management scenario.

From a numerical point of view, 1D (one-dimensional) lake models have been built (Samal *et al.* 2009; Katsev *et al.* 2010) to assess ecosystem health, giving daily information at one point, and at a depth interval of 0.5 m for 3 years daily. They observed that the changes in the stratification regime in these waterbodies affect the water quality and the ecosystem's health, primarily based on temperature and dissolved oxygen parameters. In Crowe *et al.* (2008), one monitoring station is used to examine the chemical composition of the water and estimate transport time scales in reservoirs; the main finding was that seasonal temperature variability affects biogeochemical cycling in lakes. Rueda *et al.* (2006), using 15 temperature and light profiles taken in the reservoir throughout 1 year, show that the temporal variations of mean residence times occur not only at seasonal time scales but also at shorter scales. Several 2D (two-dimensional) models have been built to characterize thermal stratification and assess water quality. In Lindenschmidt *et al.* (2019), with monthly measurements, showed the influence of climate change on water quality reservoirs. Mesquita *et al.* (2020), Basso *et al.* (2021), Azadi *et al.* (2019) modeled and analyzed different scenarios that could cause eutrophication processes using monthly measurements. Ziaie *et al.* (2019) and Chuo *et al.* (2019) found significant differences in nutrient entrance and the relationship with algae blooms with monthly measurements. However, most works have analyzed the water quality and thermal dynamics without considering 3D (three-dimensional) processes.

1D and 2D models have the advantage that they are much faster than 3D ones when performing numerical calculations; they allow long-term simulations and are easier to calibrate and validate as they depend on fewer parameters. For example, the 1D model revealed daily air and water temperature relationships but failed when the advective term was significant. It also fails to quantify the potential effects of climate change on water temperature in a shallow reservoir (Gooseff *et al.* 2005). Note that this approach cannot predict stratification dynamics. A 2D model is essential for studying stratification dynamics subject to horizontal advection. Even though 1D and 2D models can consider short- and long-wave radiation in the thermal model, heat flux by evaporation/condensation, and the convection process at the free surface, they cannot capture the processes of heat exchanges with both the bottom and atmosphere, while the 3D does. Besides, the turbulence models have been demonstrated to be important in maintaining the thermoclines and are fully developed only for 3D models (Goudsmit *et al.* 2002).

In the case of 3D models, phenomena at multiple scales and couplings can be modeled. Other 3D flows, including gravity current, significantly affect the water quality and temperature (Kopmann & Markofsky 2000). In complex geometries with highly three-dimensional flows, the more traditional depth or width-averaged models cannot accurately capture mechanisms affecting temperature transport and mixing (Politano *et al.* 2008). Overall, 3D modeling tools are critical to understanding the interaction between all aquatic ecosystem components. 3D modeling enables a better assessment of the high complexity of the reservoir and its natural cycles.

Regarding 3D modeling, there are several studies for shallow reservoirs, such as study of the influence of cold fronts on the heat fluxes and thermal structure in a tropical reservoir (Curtarelli *et al.* 2013), study of the circulation patterns in a shallow tropical reservoir (Yang *et al.* 2019), study of saline intrusion (Laval *et al.* 2005). However, while numerous studies have been conducted to characterize thermal stratification in temperate lakes and oceans, there have been fewer numerical studies of temperature dynamics in tropical reservoirs (Politano *et al.* 2008).

3D modeling has proven to be a valuable tool to advance the understanding of the physical processes of fluid dynamics and water quality, thermal processes such as the effects of wind and temperature induced flow (Matta *et al.* 2017), the effect of the wind and tidal forcing (Moloney *et al.* 2016), thermal discharge released to coastal areas (Gaeta *et al.* 2015, 2020), coupling with complex water quality process (Piccioni *et al.* 2021). It has also been used to assess environmental impacts from cooling and heating power plant production (Ligier & Okumura 2019), to analyze flood and ebb events and analyze indicators of the contamination degree (da Silva *et al.* 2021), to evaluate *Escherichia coli* development scenarios (Bedri *et al.* 2013), to study the dynamics of geomorphological features (Lisboa & Fernandes 2015), or the heating impact of a reservoir on downstream water temperature (Jiang *et al.* 2018; Plec *et al.* 2021). However, all these simulations have been performed without heat exchange with the atmosphere and not for tropical reservoirs.

Other 3D models use a simplified heat exchange model (Scanlon *et al.* 2020) to assess the climate change scenario's impact over a small tropical lake (Duarte *et al.* 2021), to evaluate the impact in coastal areas, simulate flooding and hydrodynamic patterns in wetlands (Costi *et al.* 2019), and to study thermosaline circulation in an estuary (Vouk *et al.* 2019). However, as explained by Politano *et al.* (2008), these studies are not performed on tropical reservoirs, and other 3D models have been developed to use the entire atmosphere–water exchange considering hydrometeorological conditions (Angelotti *et al.* 2021) but without complex geometry.

Some recent studies have assessed the effects of the advection schemes and turbulence and other important numerical parameters with salinity as a tracer on 3D models (Smolders *et al.* 2015; Chen 2020; Justin-Brochet *et al.* 2021), to evaluate the non-hydrostatic 3D model in rivers (Politano *et al.* 2008), optimize numerical parameters in 3D models for the calibration in small lakes (Merkel 2019), or coastal areas (Cooper & Spearman 2017; Gaeta *et al.* 2020), but they were not used to analyze those conditions in a stratified deep tropical large reservoir with spatiotemporal data of high frequency for calibration.

Complex reservoirs such as deep tropical lakes, with elongated heterogeneous basins, with the influence of several rivers or advective flows (Marín-Ramírez *et al.* 2020), are vertically complex systems, making difficult both the building and the implementation of a model that correctly represents the thermal structure.

In this sense, the present work emerges as a response to integrating a robust water quality model that studies the effect of hydroclimatological variables such as air temperature, wind, and internal mixing process on the thermal dynamics of a tropical reservoir in Colombia, using highly resolved simulations of hydrodynamic, thermal, and energy processes. The importance of these processes has been demonstrated by data analysis from the observations of La Miel reservoir (Alzate-Gómez *et al.* 2023).

Based on the context discussed here, the study analyses thermal dynamics over the vertical water column in a tropical reservoir. The general objective of the present work paper is to show the potential and limitations of three-dimensional hydraulic models in predicting the thermal distribution of rivers with reservoirs and hydro-plants. This leads to analyze different modeling hypotheses for temperature and air–water exchange and evaluate the model performances on short periods according to the observations. Section 2 outlines the characteristics of the study site. Then, Section 3.1 presents the available data. Section 3.2 describes the governing equations, and Section 3.3 details the model that has been implemented along with the performance criteria. Finally, Section 4 describes the results, and a discussion of the main findings is given in Section 5.

2. DESCRIPTION OF THE STUDY AREA

The study comprises the Amaní Reservoir, formed by the La Miel, Moro, and La Negra rivers, a hydroelectric power plant in Caldas, Colombia. The La Miel river basin is in the Central Mountain range of the Colombian Andes, specifically in the

Caldas department. The river reaches being studied have a length of 62 km and an upstream catchment area of 712 km^2. In this area, La Miel has a variety of tributaries, including Tenerife, Salado, Manso, Moro, Pensilvania, and Samaná, among others, as shown in Figure 1.

'La Miel I' dam is a gravity dam located on the riverbed (see Figure 1) and was built between 1997 and 2002 for hydroelectric power generation. The tropical reservoir Amaní (5.25° lat, −75° lon) is upstream of the dam. The dam is 188 m high, giving it a storage capacity of 571 million m^3 and a surface area of 12.2 km^2 with a generation installed capacity of 396 MW in three turbine units. Its commercial operation began in December 2002. In 2010, the Guarino diversion dam

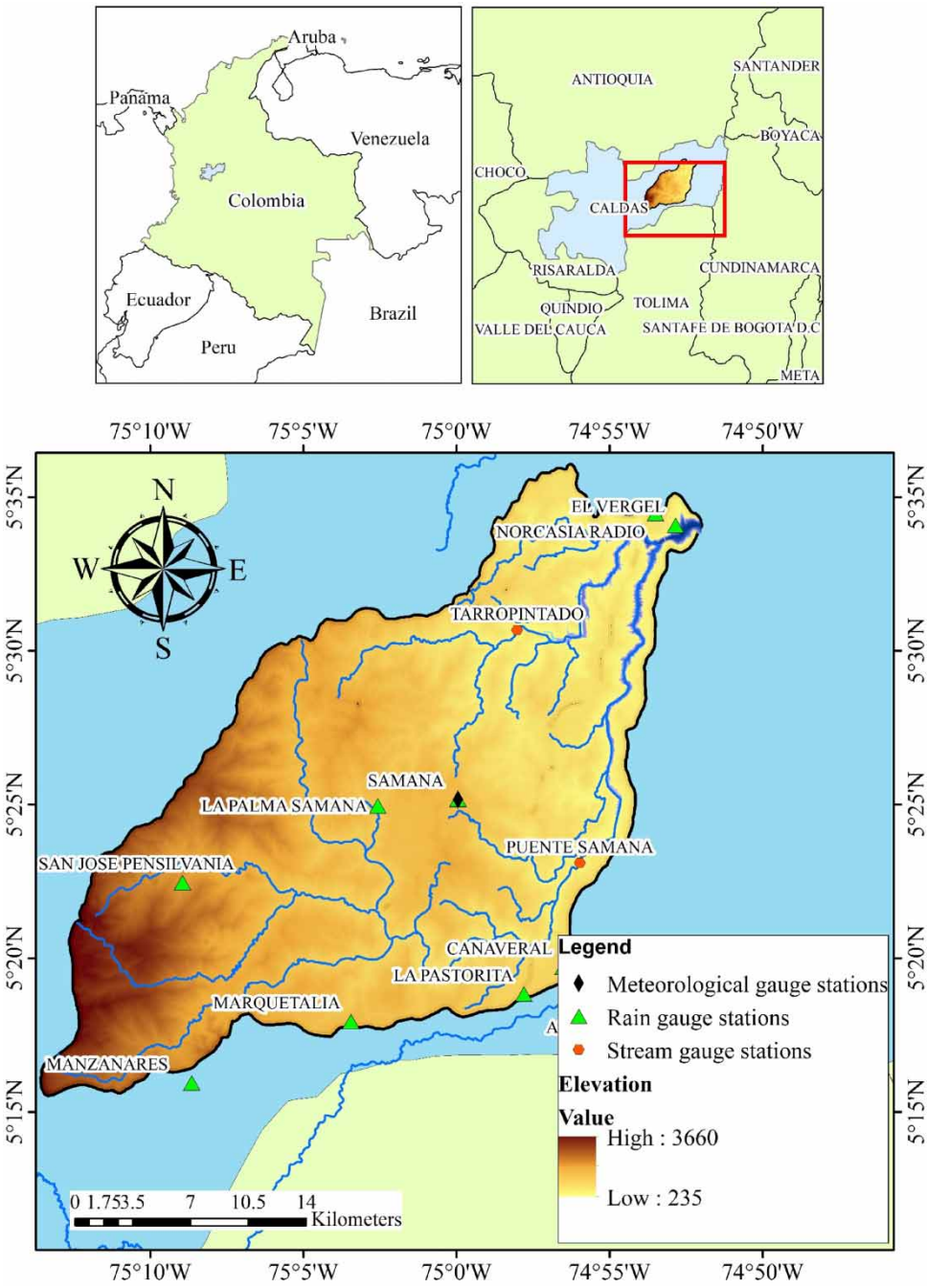

Figure 1 | Study area location and gauging stations (accessed through ASF DAAC 15 July 2015).

on the Guarino River was opened, and the Manso diversion dam on the Manso River began operations in 2013. Both divert water into the 'la Miel I' Reservoir through a tunnel.

The reservoir is located in a deep canyon and comprises two main branches: the La Miel River, 20 km long, and the Moro River, 13 km long. The maximum width is 400 m near the dam. A tiny branch is also formed by the creek Santa Bárbara, a tributary of the Moro River, the location of which is shown by the stream point in Figure 2. Amaní reservoir presents permanent thermal stratification, although its thermal structure shows seasonal variations (rainy and dry periods), with daily changes.

Analyzing the data from the meteorological measuring stations is described in Section 3.1 'Field Data and the Monitoring System': the average temperature is 25.3 °C, the maximum temperature is 33 °C, and the minimum is 18 °C. The highest monthly evaporation rates occur in the dry season, with 188 mm/day, while the lowest evaporation rates occur in the wet season, with an average of 56 mm/day. Relative humidity varied between 40 and 100%, with a mean value of 80%.

The annual cycle of rainfall in the area presents a bimodal behavior, with maximum flows in November–December and March–April and recession in July–August and January–February, with the recession in July–August being considerably more substantial. The lowest precipitation values occurred in July at 122 mm and the highest in October and November with values of 416 mm. The average flows of the La Miel and Moro rivers at the Puente Samaná and Tarro Pintado (see Figure 1 stream points) gauging stations are close to 50 and 20 m^3/s, respectively (estimates made with data from 2003 to 2016).

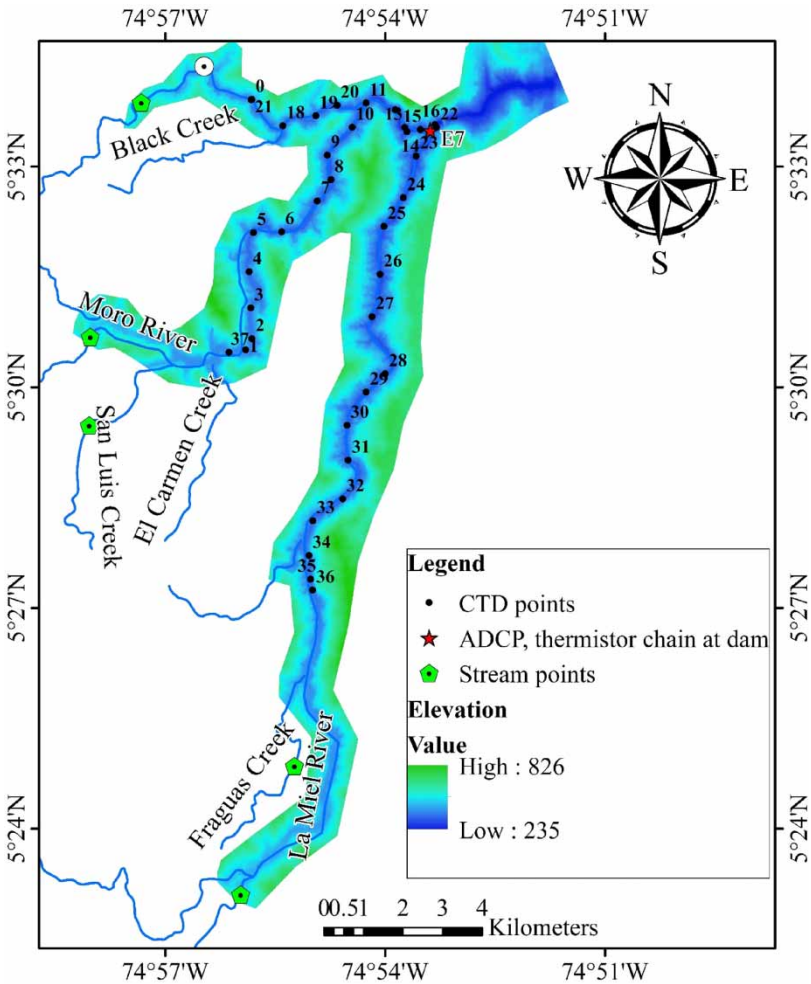

Figure 2 | Data temperature and inlet measurement's location (dataset: ISAGEN).

3. MATERIALS AND METHODS

In this work, high-frequency field data were used, 3D simulations were performed, and the former was compared with the latter. The data needed for the implementation of the model were analyzed, the mathematical equations and their implications for the modeling were analyzed, and the model configuration was adjusted accordingly as a basis for the understanding of the thermal dynamics. The hydrodynamic model was calibrated according to the observed data and the error was quantified using metrics. Then, the model responses to different thermal forcing are analyzed and the results were compared with the observed data.

The materials and methods used for this purpose and the specifications for each stage are explained in Sections 3.1, 3.2, and 3.3.

3.1. Field data and the monitoring system

The monitoring system comprises water quality measurements at five stations, of which only the E7 station next to the dam will be used, in addition to thermistor chains and CTD (Conductivity Temperature Depth) instruments. For the same period, five hydrological parameters (flow rate, precipitation, evaporation, wind, and air temperature) covering all areas of the basin have been collected; specifically, seven monitoring stations have been used to measure precipitation, two stations for flow rate and two stations for the other hydrometeorological parameters (gauging stations, Figure 1).

In station E7 as shown Figure 2, water depth with ADCP (Acoustic Doppler Current Profiler) instrument and temperature measurements were made at five different depths: two in the epilimnion (subsurface and center), one in the middle zone, and two in the hypolimnion (center and three meters from the bottom). In addition, a thermistor (Figure 2) was installed near the dam (E7) to have a continuous temperature record from April to September 2016. In addition, four thermistors were placed in this reservoir at 1.5, 4.5, 15, and 40 m depth and allow to measure the typical behavior of the temperature profile. The thermistor located at 1.5 m records the temperature of the superficial mixed layer (epilimnion), the one at 4.5 m is located approximately in the thermocline, and the one at 15 m records the temperature of the hypolimnion above the intake structure in the layer that presents the most significant temperature variations and the 40 m to capture the temperature at the bottom. All thermistors were programed to collect data every 15 min. These measurements were taken between May 2016 and September 2016.

Additionally, three field campaigns were carried out to collect temperature on about 36 profiles (CTD points Figure 2) in the reservoir and tributaries. The campaigns were carried out on the following dates: (1) 6 and 7 July, 2015 (monthly monitoring), (2) 16 and 17 August, 2015, and (3) 22 September, 2015. Vertical measurement profiles were taken at different reservoir points using a master CTD RBR profiler with temperature, turbidity, conductivity, and chlorophyll sensors. This equipment allows data to be taken with a frequency of 6 Hz along the vertical profile line. The obtained profile shows a resolution of about 5 cm.

Hydrological parameters were collected hourly for 183 days from 20 May, 2016 to 30 September, 2016 (El Vergel gauging station, Figure 1). Hydrometeorological data were obtained from the DHIME website (http://dhime.ideam.gov.co/atencion-ciudadano/) of the Institute of Hydrology, Meteorology and Environmental Studies (IDEAM, acronym in Spanish). The meteorological information used for the model was provided from the gauging station closest to the dam.

Some missing data as flow discharge from the other tributaries, Santa Bárbara, San Luis, and Fraguas, and water temperature for all the tributaries, were calculated from the SWAT (Soil and Water Assessment Tool (Gassman *et al.* 2007)) model (see Figure 2 stream points). SWAT is a semi-distributed and physically based model for daily simulation of daily discharge, sediments, nutrients, and water quality parameters. The most critical processes simulated by the model are surface runoff, infiltration, lateral flow, base flow, evapotranspiration, and groundwater recharge (Tessema *et al.* 2021). The model was calibrated using daily discharges from the Puente Samaná and Tarro Pintado gauging stations from 1985 to 1990 and validated from 1990 to 1997.

For the hydrodynamic model, topographic and bathymetric information was used, condensed in a digital terrain model (DTM) built with bathymetries of the river collected between 2015 and 2016, with a resolution of 5 m × 5 m (Figure 2). Figures 3–7 show the temporal evolution of some field data collected during 2 months, August and September 2016, at the El Vergel measuring station shown in Figure 1, for 2 months in August and September 2016. The hourly air temperature data from the El Vergel meteorological station near the dam were analyzed (Figure 3), and the monthly variations were minor. Figure 3 shows a cycle evolution, where the lowest temperatures are marked in the early morning (4 am) and the highest in the afternoon (3 pm). During the study period, the minimum temperature was 19.6 °C, the average temperature was 26 °C, and the maximum temperature was 35.1 °C.

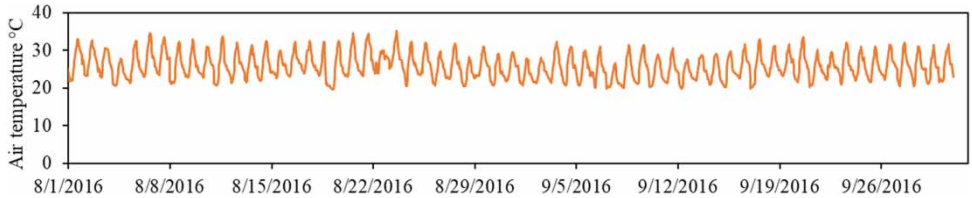

Figure 3 | Air temperature at the gauging station El Vergel, used as input on the thermic model.

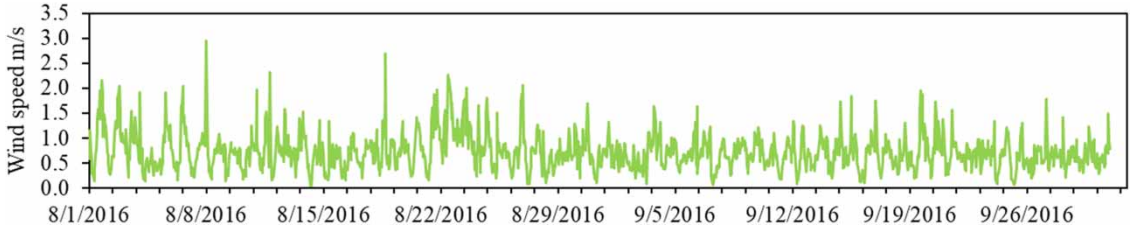

Figure 4 | Wind speed at the gauging station El Vergel used as input on the thermic model.

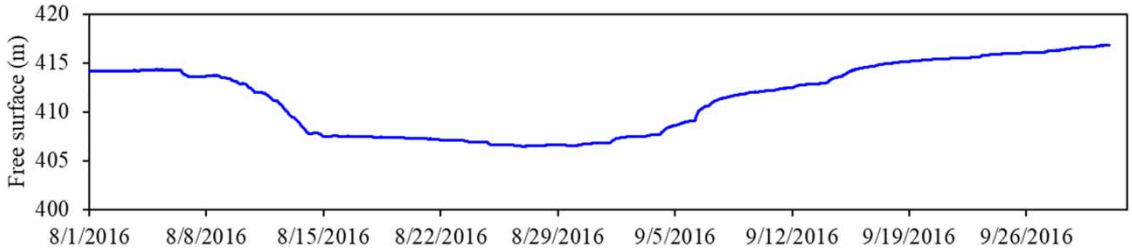

Figure 5 | Water level at the dam used as observation for calibration of the hydrodynamic model.

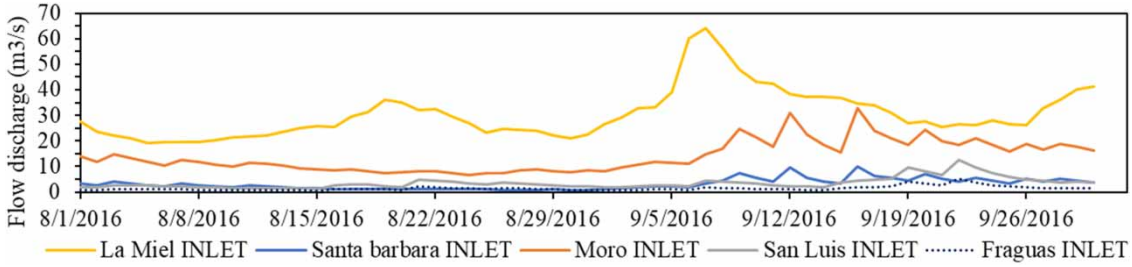

Figure 6 | Inlet flow or boundary condition on the hydrodynamic model correspond to stream points in Figure 2.

In Figure 4, the wind speed data are presented. During the study period, the minimum wind was 0.05 m/s, the average wind was 0.73 m/s, and the maximum was 3.0 m/s. The canyon topography of the area reservoir may explain the low wind speed values. The reservoir operated at a low water level in August, and the water level varied by 7 m, reaching 406.5 m on 27 August. The water level remained like this for 2 weeks, then rose again until it reached 417 m by the end of September (Figure 5). The inflow remained roughly constant during August, at 25 m^3/s into Miel, except at the beginning of September, where the peak flow was as high as 65 m^3/s in La Miel's arm. The reservoir presents indeed more inflow from the La Miel arm, as seen in Figure 6.

Figure 7 shows the water temperature for each tributary of the Amaní reservoir. For the La Miel river, the average temperature is 23 °C. The creek Fraguas contributes to the river La Miel and presents an average temperature of 24 °C. The Moro River has an average temperature of 25.5 °C. San Luis, a tributary of the Moro, presents an average temperature of 24 °C. Santa Bárbara Creek presents an average temperature of 23.8 °C. Figure 8 presents the high-frequency measurement of the vertical temperature profile at the dam location from 1 August to 22 September, 2015. Again, there is a permanent stratification in the reservoir: slightly significant differences are observed on the hourly and daily scale and non-very significant on the monthly time scale.

The water temperature distribution in the analysis process presents no mixing phenomenon, and there are at least six layers in August–September. The layers that present the most significant variation are in the first meters up to 10 m. The temperature distribution of the first four layers varies greatly, while the temperature distribution of the two deepest layers does not change much. Also, the high-resolution data suggest that stratification does not breakdown overnight.

The vertical structure of water temperature is stable in different periods of each month, and the surface temperature is relatively high throughout the year, with a mean value of 29.6 °C and a maximum of 31.8 °C at the free surface. At depths between 25 and 15 m, the temperature in the reservoir appears moderated by the temperature entering the tributaries. The temperature in the deep layers is between 22 and 23 °C. The analysis in the next section indicates that the external heat flux, which is determined by meteorological and inflow conditions, is insufficient for altering the nearly stratified state of the reservoir.

Clearly, there is a permanent stratification in the reservoir: hourly and daily fluctuations of the isotherms 28, 29, and 30 °C in the epilimnion (of about 1–3 m) are observed. On the monthly time scale, we also observe an overall increase of the temperature of about 2 °C in the dam followed by a decrease of similar intensity, as the isotherms plunge by about 5 m and get back to their initial location.

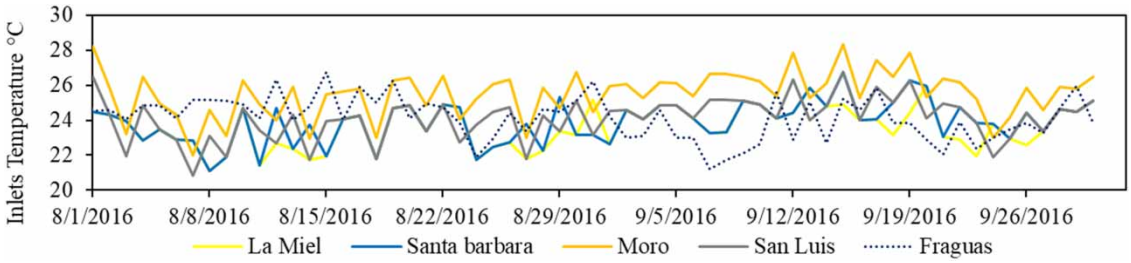

Figure 7 | Water temperatures at the tributaries or boundary conditions used as input on the thermic model.

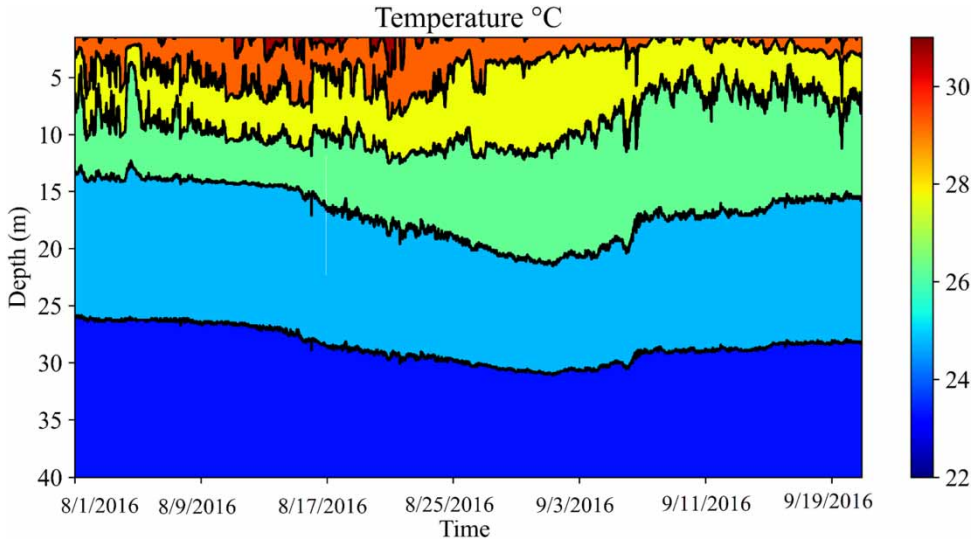

Figure 8 | Evolution of the vertical distribution of the temperature using four sensors on a rope at the dam.

One of the critical factors in the formation of the thermal structure is the surface heat flux, which is composed of solar radiation, incident and emitted long-wave radiation, sensible heat flux, and latent heat flux. Often, this energy flow results in an increase in the temperature of the surface layer of the reservoir and, thus, a decrease in its density. In contrast, the deeper layers remain cooler because they are less exposed to these heat sources as shortwave radiation penetration is limited, and diffusive heat transport is too slow, as seen in the measurements (Figure 8). In the tropics, the absence of seasons means that the difference between maximum and minimum annual radiation is slight. In addition, the total daily radiation is remarkably constant throughout the year since there are no significant variations in the number of daylight hours per day. This lack of variation in the daily radiation received means that surface heat fluxes do not vary so dramatically, and therefore, monthly patterns of stratification and mixing are not very pronounced in the present case.

From August to September, some variations in the reservoir temperature appear due to changes in the inflow and outflow of water, especially the difference in the operation level of the reservoir and meteorological conditions. Hence, the water temperature stratification pattern slightly differs from August to September as shown Figure 8.

3.2. Governing equations

In order to achieve the objectives outlined, it is necessary to have a 3D model of coupled hydrodynamics and temperature, which must be validated to ensure that what is simulated is representative compared to observed behavior.

For the hydrodynamic component, the code solves three-dimensional hydrodynamics equations with a coupled energy equation regarding temperature. The equations presented were obtained with the following assumptions (Hervouet 2007):

- Three-dimensional equations of incompressible flow with a free surface changing in time (Equations (1) and (2)),
- Negligible variation of density in the conservation of mass equation (incompressible fluid),
- Hydrostatic pressure (Equation (3)),
- the Boussinesq approximation (Equation (6)) for the momentum (the density variations are only considered in the buoyant forces).

Due to these assumptions, the three-dimensional equations (mass and momentum) being solved are (Equations (1) and (2)):

$$\nabla \cdot \boldsymbol{U} = 0 \tag{1}$$

$$\frac{\partial U}{\partial t} + U \cdot \nabla U = -\frac{1}{\rho_0} \nabla p + \frac{1}{\rho_0} \nabla \cdot (\mu_{\text{eddy}}(\nabla U + {}^{t}\nabla U)) + g + F \tag{2}$$

The hydrostatic pressure assumption is (Equation (3)):

$$\frac{\partial p}{\partial z} = -\rho g \tag{3}$$

where the density can be decomposed as in Equation (4):

$$\rho = \rho_0 + \Delta\rho \tag{4}$$

Giving the following expression of Equation (5) for the hydrostatic pressure:

$$\frac{\partial p}{\partial z} = -\rho_0 g\left(1 + \frac{\Delta\rho}{\rho_0}\right) \tag{5}$$

Finally, when the Boussinesq approximation is considered, the pressure expression will be as in Equation (6) (TELEMAC-3D 2020):

$$p = p_{\text{atm}} + \rho_0 g\,(Z_s - z) + \rho_0 g \int_z^{Z_s} \frac{\Delta\rho}{\rho_0}\, dz' \tag{6}$$

Here, U (m/s) indicates the three-dimensional component of velocity, t (s) indicates the time, ρ (kg/m^3) indicates the density, ρ_0 (kg/m^3) indicates the reference density, g (m/s^2) indicates the acceleration due to gravity, p (Pa) indicates the pressure, F (m/s^2) represents the external forces, h (m) indicates the water depth, Z_S (m) indicates the free surface elevation, p_{atm} (Pa) indicates the atmospheric pressure, μ_{eddy} (m^2/s) indicates the eddy viscosity, x, y (m) indicate the horizontal space components, z (m) indicates the vertical space component.

To solve temperature, coupled with hydrodynamics, this study uses the evolution of the water mass temperature is derived through the evolution equation of internal energy. TELEMAC-3D can be directly coupled (two-way coupling) with the WAQTEL module on the same computational mesh to reproduce the thermal dynamics. The thermic model WAQTEL (version 8.2) computes the water mass temperature through the evolution of internal energy (Equation (7)) with $E =$ internal energy (J), $\lambda =$ thermal conductivity (W.m^{-1}. °C^{-1}), with $T =$ water temperature (°C), and S_{surf} (W/m^2) the surface sources, which are the exchange fluxes through the free surface (WAQTEL 2021). The internal energy is formulated as a function of temperature T, considering that the internal energy E is expressed as formulated in Equation (8). As thermal diffusivity is the thermal conductivity divided by density and specific heat capacity at constant pressure, the resulting equation is, therefore, presented in Equation (9):

$$\frac{\partial E}{\partial t} + \boldsymbol{U} \cdot \nabla E - \nabla \cdot (\lambda \nabla T) = \frac{S_{\text{surf}}}{h} \tag{7}$$

$$E = \rho C_p T \tag{8}$$

$$\frac{\partial T}{\partial t} + \boldsymbol{U} \cdot \nabla T - \nabla \cdot (\alpha \nabla T) = \frac{S_{\text{surf}}}{\rho C_p h} \tag{9}$$

where C_p is water-specific heat (J/kg°C) and ρ (kg.m^{-3}) is the water density, α is the thermic diffusivity coefficient (m^2/s). The coefficient of turbulent diffusion (or dispersion) k_T is added to the diffusivity coefficient, which can generally be neglected as the value is low, which lead to Equation (10):

$$\frac{\partial T}{\partial t} + \boldsymbol{U} \cdot \nabla T - \nabla \cdot (k_T \nabla T) = \frac{S_{\text{surf}}}{\rho C_p h} \tag{10}$$

The linearized formula of the balance of heat exchange fluxes at the free surface is used to represent the interchange between water and atmosphere, where the thermal power liberated into the atmosphere per surface unit, denoted as Φ, is assumed to be proportional to the difference in temperature (T–T_{air}) where T_{air} is the air temperature. So, $\Phi = A\ (T\text{–}T_{\text{air}})$, where A is the exchange coefficient in W/m^2/°C. The heat flux leaving the water domain is (Equation (11)):

$$\Phi = -\rho C_p k_T \nabla T \cdot n = \rho C_p k_T \frac{\partial T}{\partial z} \tag{11}$$

with $\boldsymbol{n}$ the average vector pointing outward the free surface and k_T the molecular heat diffusion coefficient in water in m^2/s. Then, equating the two formulations of Equation (11) leads to the boundary condition at the free surface (Equation (12)):

$$k_T \frac{\partial T}{\partial z} = -\frac{A}{\rho C_p}(T - T_{\text{air}}) \tag{12}$$

Note that A includes radiation, air convection in contact with water, and latent heat from evaporation. It is here modeled as in Hervouet (2007) (Equation (13)):

$$A = (4.48 + 0.49\text{T}) + 2021.5b(1 + V_{\text{wind}})(1.12 + 0.18T + 0.00158T^2) \tag{13}$$

The parameter b depends on the location site and will be calibrated in this work, V_{wind} is the wind velocity (in m/s), and T is the water temperature at the free surface in °C.

3.3. Model setup

The unstructured mesh comprises 4.779.814 nodes and 8.909.098 triangular elements with a minimum size of 0.7 m in a 2778.4 km^2 area, created with the software Blue Kenue. The mesh is made of prisms representing the spatial variations in the surface area. The model mesh is developed as a series of planes between the bed and the free surface. Twenty-three planes are used to describe the water column. These layers have a percentage distribution of 10 m at the bottom to 0.5 m near the free surface. It is a classical sigma transformation that follows the shape of the terrain (TELEMAC3D 2020).

A mesh independence test was performed, varying the size until the changes in the results were small enough not to compromise the accuracy of the simulations. The test was performed on several geometries with longitudinal variations ranging from 50 to 500 m, 20 to 400 m, 10 to 300 m, 2 to 200 m, 0.7 to 160 m, 0.5 to 140 m, and 0.1 to 35 m. Figure 9 shows the geometry from 0.7 to 160 m was finally chosen as the best compromise.

Considering that the study focuses on the sub-daily temperature variations and that the hydrodynamics do not change significantly, it is assumed that the hydrodynamic model conditions are stationary. In contrast, the conditions for the thermic model are transient. A constant water level of 410 m above the sea level measured on 6 July, 2015, is used as the initial condition for the hydrodynamic model. A warm-up time is needed to obtain a velocity field until the velocity components are developed within the computational domain. The hydrodynamics boundary conditions are as follows. First, this research imposes the flow rate at the upstream part of all the rivers using the collected field data ($Q_1 = 9.91$ m^3/s, $Q_2 = 4.96$ m^3/s, $Q_3 = 6.97$ m^3/s, $Q_4 = 6.91$ m^3/s, $Q_5 = 2.87$ m^3/s), and the turbine water or intake was added as a source, with a constant value of -32 m^3/s at a depth of 380 m above the sea level. Then, the lateral boundaries were set as closed walls with slip conditions. Their location is shown in Figure 10. For the thermic model, the initial condition is as shown in the Figure 11 of the whole computational domain was constructed from the field measurements of the CTD of 6th July 2015 at station E7.

As boundary conditions this research imposes a constant temperature at the inflows (of $T_1 = 22.9$ °C, $T_2 = 22.6$ °C, $T_3 = 24$ °C, $T_4 = 23.4$ °C, and $T_5 = 23$ °C) (see Figure 10). The boundary condition imposed on the free surface was Dirichlet for one case study and Newman for the other (Equation (12)), using air temperature, wind direction, and velocity based on data collected from the local and nearby weather stations. These approaches are developed in detail in Section 4.2.

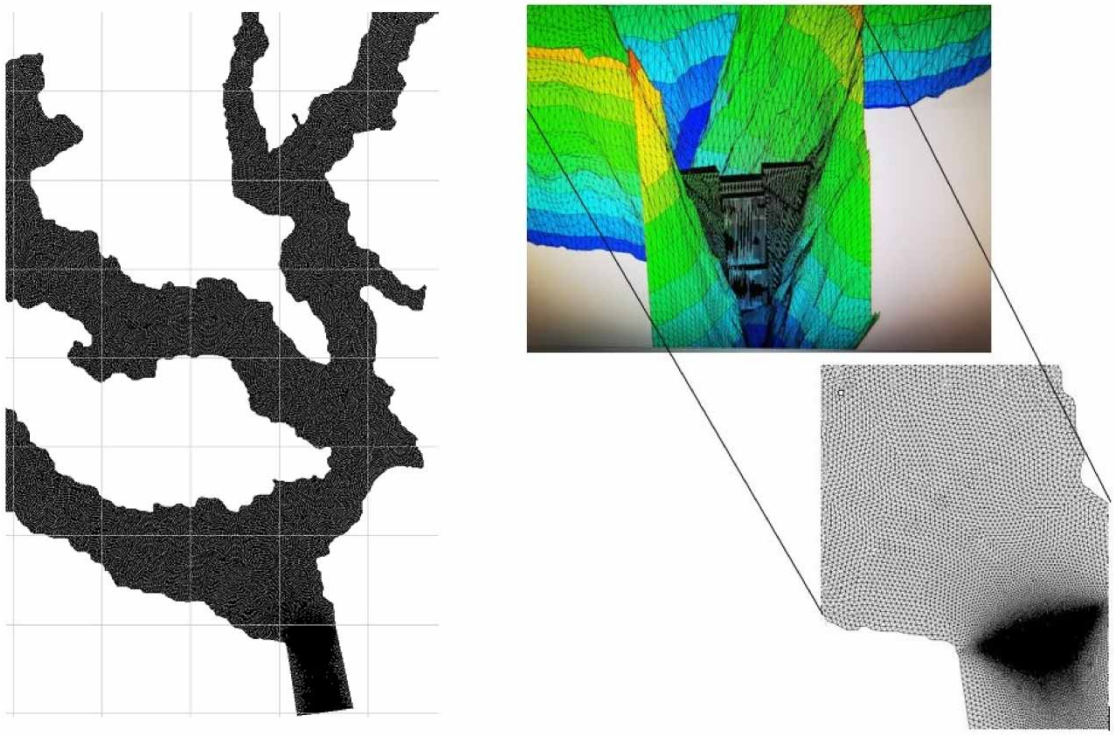

Figure 9 | Mesh used in the model. Left: general structure of the mesh in the reservoir. Right: detail of the geometry and mesh at the dam location.

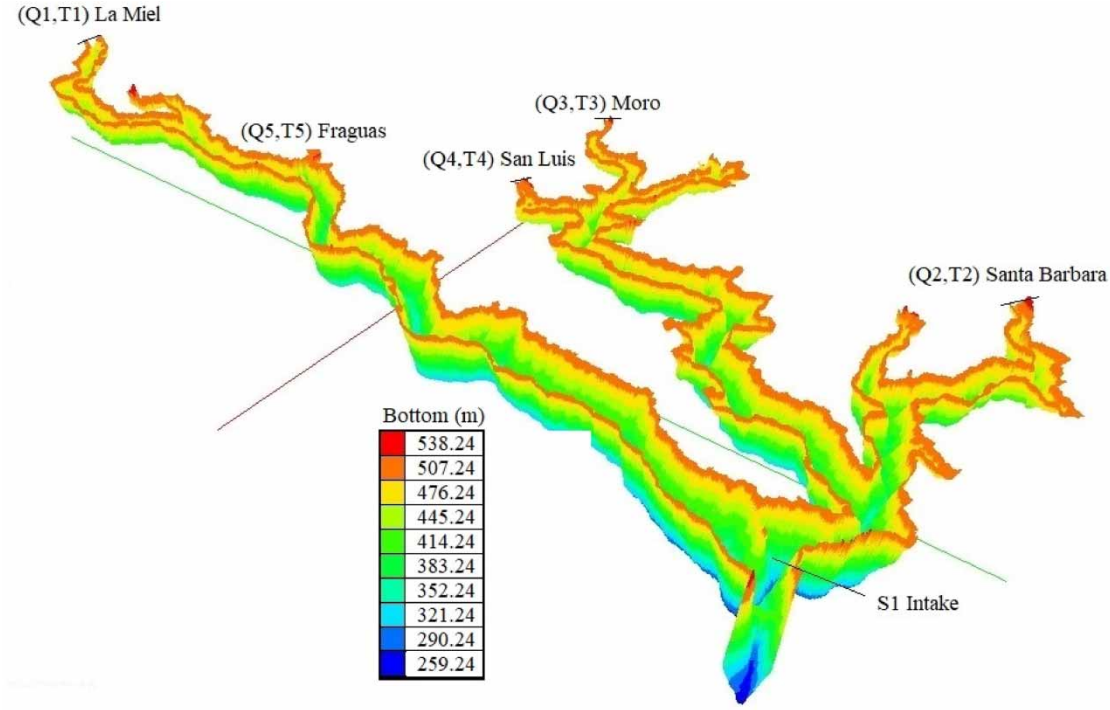

Figure 10 | Numerical setup and boundary conditions used. 3D view of the bathymetry.

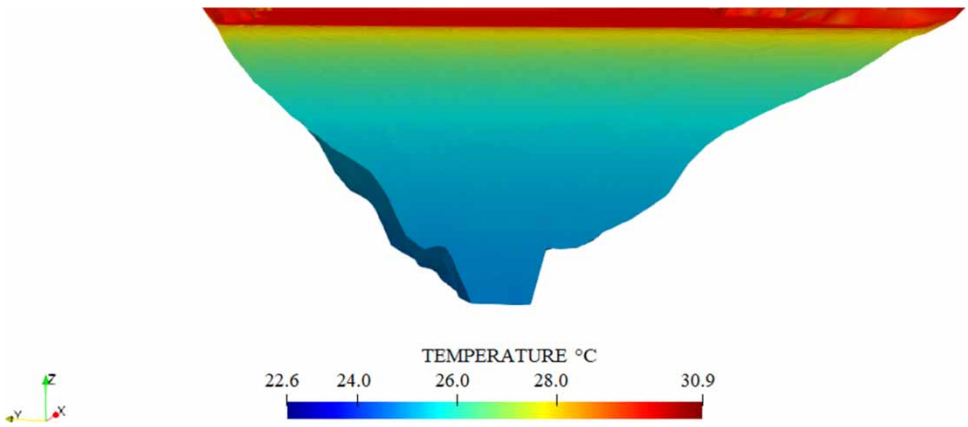

Figure 11 | Thermic initial condition near the dam at station E7.

The modules employed were TELEMAC-3D-WAQTEL version v8p2 (TELEMAC-3D 2020). The simulations were conducted for each case investigated through parallel computing on the supercomputer OLYMPE from the CALMIP computing center for public research in Toulouse. The numerical parameters were defined by trial-and-error, where the model was run several times and yielded the following results. The set of selected numerical and physical parameters is summarized in Table 1.

To solve all processes, including hydrodynamics and thermals, the GMRES solver was chosen based on mass conservation and computational cost. To simulate all the physical processes, this study uses a constant viscosity model for the turbulence model (Hinkelmann 2005; Hervouet 2007). The turbulent viscosity value was fixed at 10^{-3} m^2/s in all directions, as a results of previous simulations using Smagorisky as a turbulence model. Several simulations were run for a time step ranging from 0.1 to 5 s. The time step was set to 1 s since it provided the best compromise between stability and performance.

Table 1 | Parameters used in the calibration of the hydrodynamic model

Parameters	Value
Scheme for advection of temperature	EXPLICIT SCHEME + MURD N SCHEME
Linear solvers	
Solver	GMRES
Krylov subspace	4
Turbulence	
Vertical turbulence model	CONSTANT VISCOSITY
Horizontal turbulence model	CONSTANT VISCOSITY
The coefficient for horizontal diffusion of velocities (m^2/s)	0.001
The coefficient for vertical diffusion of velocities (m^2/s)	0.001
Law of bottom friction	STRICKLER LAW
The friction coefficient for the bottom	30

The Multidimensional Upwind Residual Distribution (MURD) method was applied for the advection of three-dimensional variables under TELEMAC-3D, and the boundary conditions were applied following the method of characteristics. The advection of tracers was solved using the distributive MURD N method. Section 5 discusses the parameter choice.

3.4. Model validation

The model's calibration and validation were done by comparing the modeled results with the field measures, especially the variation of the water level and the temperature profile at several points and in time with high-frequency data at the dam (station E7). This comparison is the first indication that the model represents a hydrodynamic and thermal stratification. Traditionally, estimated standard errors have been used to measure the efficiency of model calibration. The most common indices to analyze time-dependent variables are the mean absolute error – MAE (Equation (15)), Nash–Sutcliffe index (Equation (16)), and root mean square error – RMSE (Equation (17)) and relative error (Equation (18)):

$$\mathrm{MAE} = \frac{1}{n}\sum_{i=1}^{n}|\widehat{X_i} - X_i^o| \tag{14}$$

$$E_f = 1 - \frac{\sum_{i=1}^{n}(\widehat{X_i} - X_i^o)^2}{\sum_{i=1}^{n}(X_i^o - \overline{X^o})^2} \tag{15}$$

$$\mathrm{RMSE} = \sqrt{\frac{1}{n}\sum_{i=1}^{n}(\widehat{X_i} - X_i^o)^2} \tag{16}$$

$$\mathrm{Re} = \sum_{i=1}^{n}\frac{|\widehat{X_i} - X_i^o|}{X_i^o} \times 100 \tag{17}$$

In the equations, n is the sample size, $\widehat{X_i}$ is the predicted value of the output (water level or temperature) at time or location i, X_i^o is the corresponding measured value, and $\overline{X^o}$ is the mean of the measured values.

The MAE and RMSE have been used as standard statistical metrics to measure model performance in meteorology, air quality, and climate research studies. The difference is that the MAE gives equal weight to all errors. At the same time, the RMSE penalizes the variance, giving more weight to errors with larger absolute values than to errors with smaller absolute values. As a result, when both metrics are calculated, the RMSE is never lower than the MAE (Chai & Draxler 2014).

Another critical aspect of the error metrics used for model evaluations is their capability to discriminate among model results. In this case, the advantage of the Nash–Sutcliffe index is that it can be applied to a variety of model types. This efficiency index ranges from $-\infty$ to $+1$, 1 being the best. As well as RMSE and MAE, the Nash–Sutcliffe is a helpful index; however, it can be sensitive to several factors, including sample size, outliers, magnitude bias, and time-offset bias. So, using a combination of those indexes to assess the model is better. These statistics are commonly used to evaluate the model's goodness that fits the observed data (Lindim *et al.* 2011; Amorim *et al.* 2021).

3.5. The three scenarios of temperature forcing

Considering that the model is very sensitive to the temperature forcing given by the atmosphere–water exchange, it is necessary to analyze the thermodynamic behavior of the exchange process concerning the different forcings. Based on this, the following approaches are defined for the temperature boundary condition at the free surface:

A. A constant water temperature T_{water}, of 29.8 °C, at the free surface (Dirichlet) without exchange with the atmosphere, considering the stability of the thermal stratification according to field measurements. The approach A was simulated until a steady state was reached. This approach served as initial conditions and reference for comparison with the other approaches.
B. Exchange with the atmosphere at the free surface boundary condition (Equation (12)) with meteorological forcing (air temperature T_{air} and wind velocity V_{wind}) constant in time. A value of 32 °C is imposed for T_{air} based on the maximum value measured for the day of the analysis. $V_{wind} = 0.6$ m/s refers to the mean value over the period.
C. Exchange with the atmosphere at the free surface boundary condition (Equation (12)) with meteorological forcing changing over time. This last approach uses observed hourly data of T_{air} and V_{wind} over the period.

The proposed approaches simulate the temperature profile in the reservoir under different forcings and parameters that best represent tropical conditions. They will be compared with the field thermistor data covering the period from 11 August to 19 August, 2016.

The same boundary conditions concerning the flow, source or intake, and tributaries temperature were set up for the three approaches; they have been detailed in Section 3.3.2 'Initial and boundary conditions'. These approaches were chosen for the sake of simplicity (number of parameters), data availability, and computation time.

4. RESULTS

4.1. Hydrodynamics

In this section, this study compared observation and simulation of the water level and velocities within the computational domain. The chosen period for the calibration was from 1 August until 1 September, 2016. For this period, observed data are available daily. The measurement water level at point 16 is used for calibration purposes. The results of the TELEMAC-3D model calibration exercise are presented in Figure 12, where comparisons of the water level simulations with observations are presented within each 7 days' interval. The statistical calibration indices found for the simulations show good performance with $E_f = 0.95$, MAE = 2.46 m and RMSE = 3.22 m. In order to analyze the spatial performance of the model, a correlation graph between the simulated water depth and the measured water depth was produced at 37 points

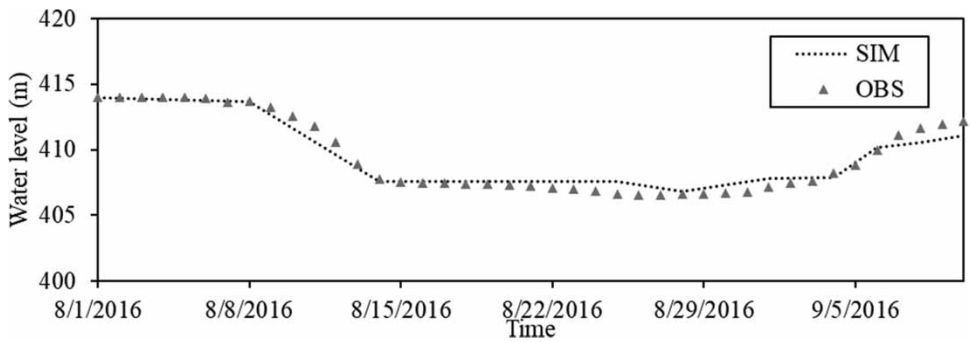

Figure 12 | Time evolution of the water level at point 16 corresponding to the dam location (Figure 2).

inside the reservoir, as shown in Figure 13. According to Figure 13, the hydrodynamic model is adequately configured since the observed water depths correspond to the simulated values in TELEMAC-3D, with an R^2 close to 1.

As expected, the order of magnitude of scalar velocity is lower inside the reservoir, and the velocity is highest at the inlets as shown in the Figure 14. The order of magnitude of the velocities ranges from 0.1 to 0.9 m/s, with the highest velocities occurring at the inlets. It is the lowest near the dam and ranges from 0.001 to 0.01 m/s. In the same way, it can be observed in Figure 15 that the velocity decreases in the vertical direction, with the highest velocity in the upper layers. Low velocities in the lower layers may indicate that there is little potential for convective transport near the bottom of the reservoir, making convection less likely to occur than in the upper layers. Therefore, convection can exist in the upper layers, but in the other layers, the process is probably reduced to diffusive transport.

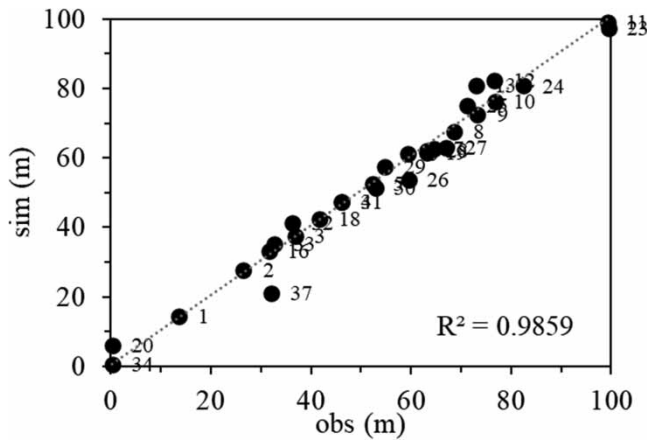

Figure 13 | Water height (in meters) at all the points displayed in Figure 2 for 17 August 2016 with CTD.

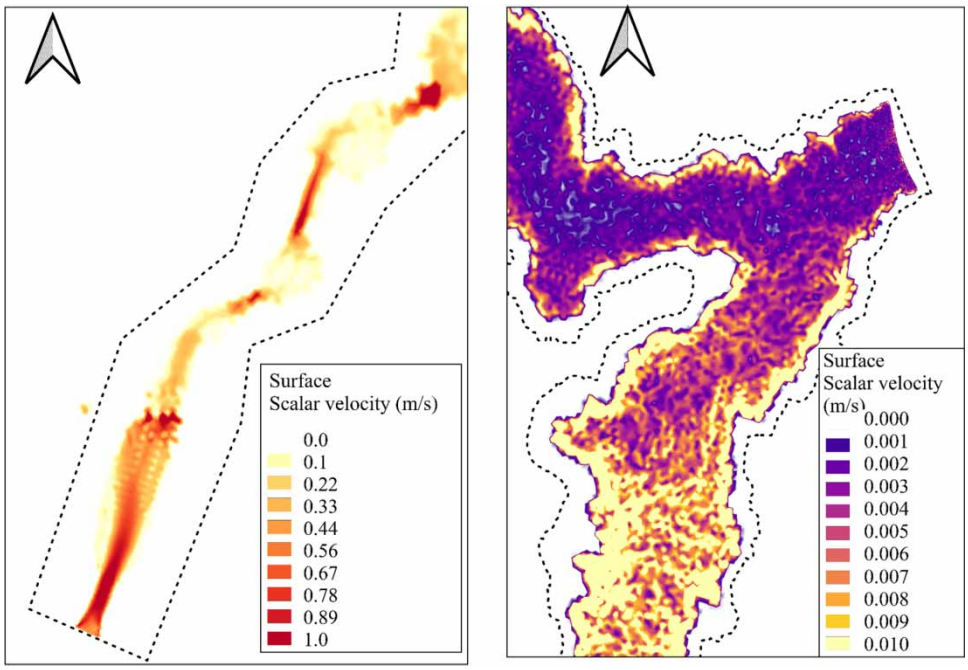

Figure 14 | Free surface scalar velocity at La Miel river entrance (left) and at the dam (right).

4.2. Thermics

The results of the temperature model for the three approaches mentioned in Section (3.3.5), which differ in the way they treat the water–atmosphere exchange, will be presented in Section 4.2.2. Considering the model's sensitivity to the parameters of this exchange, it is necessary to perform a detailed analysis of the impact of the physical parameters of the different models.

Sensitivity analysis of the thermic diffusivity of water (k_T) and the coefficient of the atmosphere–water exchange model b is required according to the governing equations (Equations (12) and (13)) of the thermal model described in Section (3.2). Table 2 presents the values tested for these coefficients in each approach. For the local sensitivity analysis, the simulations

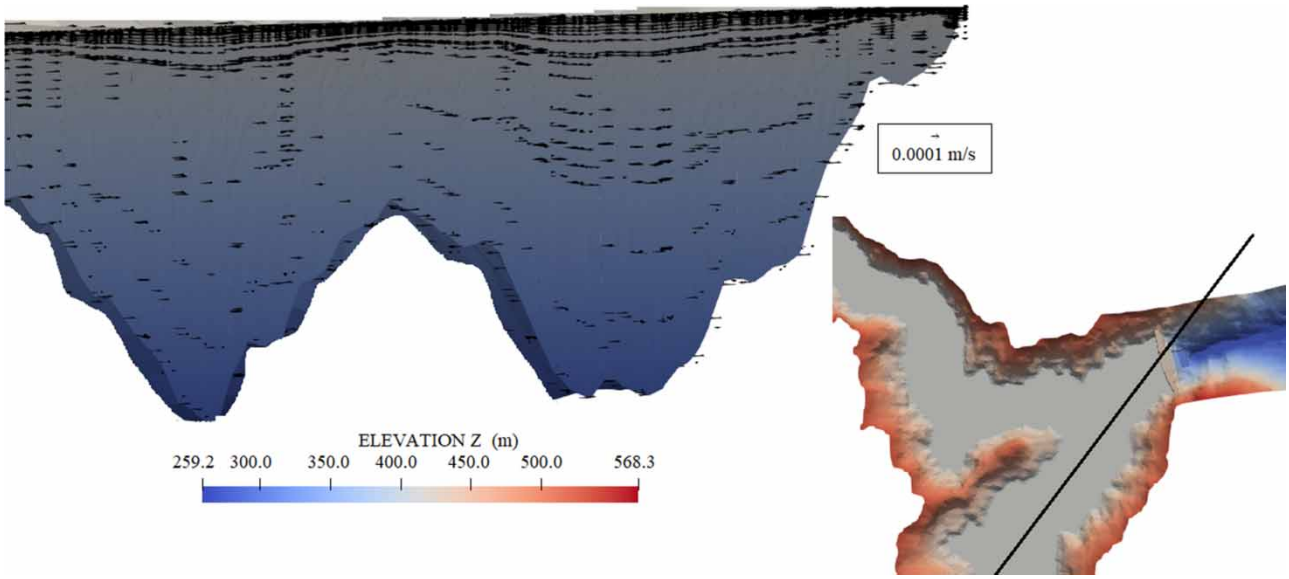

Figure 15 | Velocity field (left) along one cross-section at the dam (right) for the hydrodynamic calibration model.

Table 2 | Simulations performed in this work

Case name	Approach	b	κ_T (m^2/s)	Comment
NO EXCH 1	(A)	N/A	1.0×10^{-6}	The Prandtl number $Pr = \nu_t/\kappa_T = 1$
NO EXCH 2	(A)	N/A	1.4×10^{-7}	$Pr = 7$
NO EXCH 3	(A)	N/A	0	$Pr = \infty$
CAL0	(B)	0.0025	1.0×10^{-6}	
CAL1	(B)	0.0035	1.0×10^{-6}	
CAL2	(B)	0.01	1.0×10^{-6}	
CAL3	(B)	0.1	1.0×10^{-6}	
CAL14	(B)	0.01	0	$V_{\text{wind}} = 0$ m/s
CAL 1C	(C)	0.0035	1.0×10^{-6}	
CAL 2C	(C)	0.01	1.0×10^{-6}	
CAL 3C	(C)	0.1	1.0×10^{-6}	
CAL4	(C)	0.03	1.0×10^{-6}	
CAL5	(C)	0.05	1.0×10^{-6}	
CAL15	(C)	0.1	0	Taking as IC CAL3 last time step
CAL17	(C)	0.0025	1.0×10^{-6}	

A, B, and C refer to the scenario type (see Section 3.3 for details).

were performed using the 'one-at-the-time' approach (Rajabi *et al.* 2015) by increasing each parameter by a given percentage while leaving all others constant and quantifying the change in model output.

A sensitivity analysis was performed on thermic drivers for air–water exchange included in the simulations to define which of them primarily influenced the models' performance as being sensitive to the variation of the simulated processes.

The analysis was carried out at the four depths of the dam, where Depth 1 corresponds to the temperature at the free surface, Depth 2 corresponds to the temperature at 4 m, Depth 3 corresponds to the temperature at 15 m, and Depth 4 corresponds to 40 m. These points were selected to represent the stratification; the field measurement data used to evaluate the simulations were taken between 11 August and 19 August, 2016. A spatial assessment compared to the temperature profiles measured by the CTD for 17 August was also performed. To investigate model performance, RE, RMSE, and MAE between measured and simulated temperature values were calculated.

4.2.1. Approach A: constant water temperature at the free surface without exchange with the atmosphere

Approach A: the analysis was applied to the different drivers included in the simulation, as listed in Table 2, considering the thermal diffusivity (k_T) of water for three runs. The influence of the simulated processes strongly depends on the investigated location's depth in Figure 16. In particular, points evaluated in Depth 2 present the highest errors in the case NO EXCH 1, ranging between 14.2% RE, 4.4 °C for RMSE, and 4.1 °C for MAE. When the thermic diffusivity of water was zero (NO EXCH 3), the simulations reported better results. Hence, heat transfer is favored to occur by fluid momentum rather than by fluid conduction. The results are discussed in detail in the next paragraph.

Observed and simulated water temperatures at the four depths during the analysis period are presented in Figure 17, showing the difference between the surface and bottom layers for measured and simulated water temperature.

According to Figure 17, the model could represent the main observed patterns, the first layer being the constant water temperature boundary condition at the free surface: (i) the second layer shows a slight observed variation in temperature between 28.0 and 31.41 °C for the period at an hourly scale. At 4 m after a transition period, NO EXCH 1 and NO EXCH 2 exhibit almost the same results with an increase of temperature which is not observed, whereas NO EXCH 3 simulates a constant temperature; the same behavior appears in the simulated results at 15 m; (ii) the cooling at the reservoir bottom, shows an

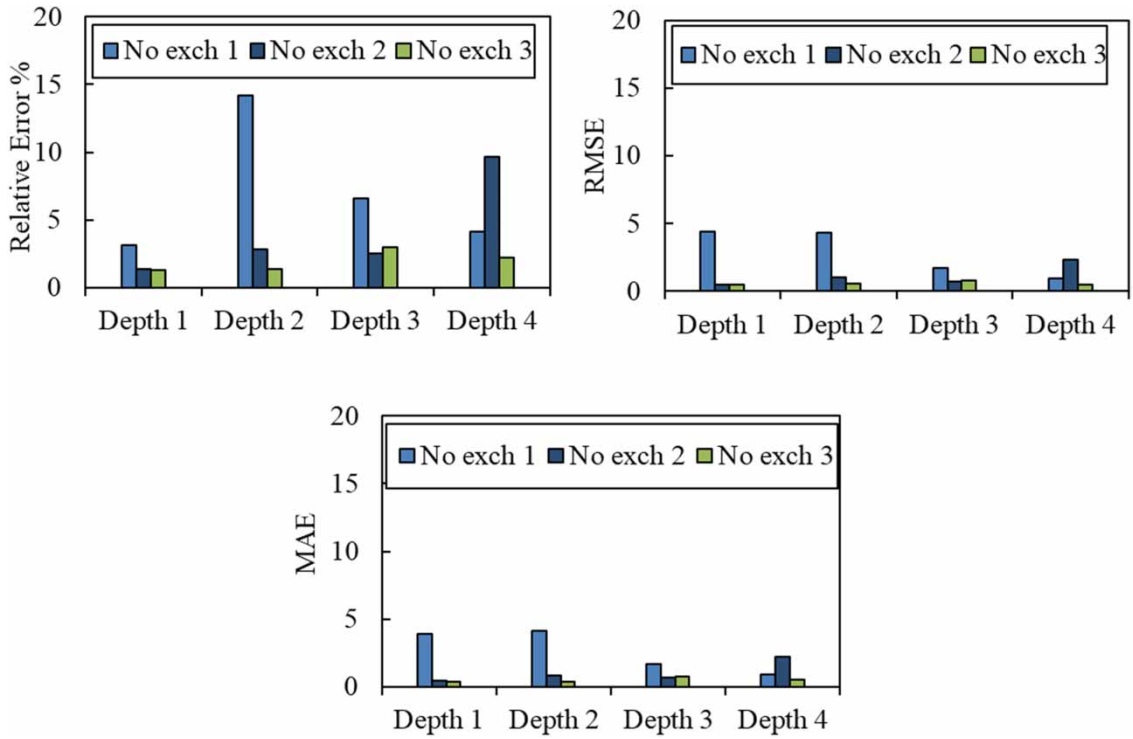

Figure 16 | Metrics for approach A, at different depths in the dam.

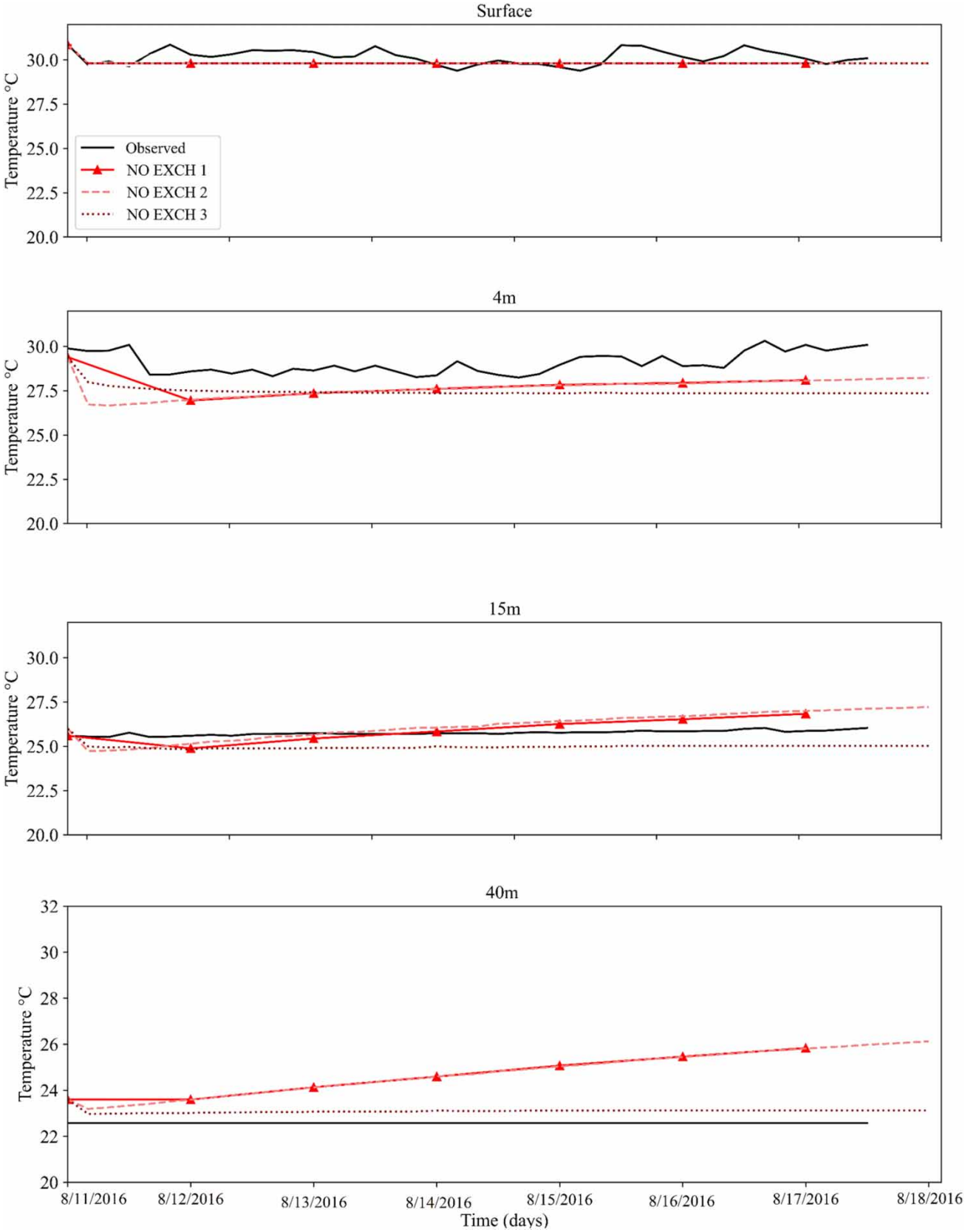

Figure 17 | Time variation of the observed and simulated temperatures at the dam without exchange with the atmosphere.

overestimate of 0.5 °C for NO EXCH 3 and more than 2 °C and increasing with time for the other cases. For the cases of NO EXCH 1 and NO EXCH 2, there is a tendency for the bottom temperature to increase, which is not representative of the current situation for reservoirs with little change over time; (iii) the duration of the stratification period that never breaks in all cases; (iv) using approach A, it was not possible to reproduce the temperature oscillations, only the mean values which is due to the constant water temperature boundary condition at the free surface.

Figure 18 shows the simulated and observed temperature profiles: vertical profiles at different points in the dam at a given time. It shows that the model can reasonably simulate the vertical stratification characteristics of the water temperature of the Amaní Reservoir, and case NO EXCH 3 is in good agreement with the observed water temperature structure of each analysis point. However, the model simulates only one thermocline, not the two that occur in the Amaní tropical reservoir. Results are very similar for cases NO EXCH 1 and 2 with an increase of temperature near the bottom: mixing phenomena are simulated, which do not represent measurement data (Figure 18 for points P20, P29, P10, and P16).

The thermal structure along the reservoir near the dam is shown in Figure 19 for case NO EXCH 3. Generally, the water temperature was not homogeneous during the analysis period. With reported air temperature values of around 28 °C during the analysis period, a warmer layer of water developed at the surface, eventually developing into a strongly stratified thermocline at two depths in 5 and 10 m, but as already mentioned it was not possible to reproduce the deeper thermocline at 10 m with approach A.

Unlike many natural lakes that experience overturning depending on weather conditions, no overturning was observed during the study at Amani Reservoir because it is a tropical lake, and the surface water temperature never drops below

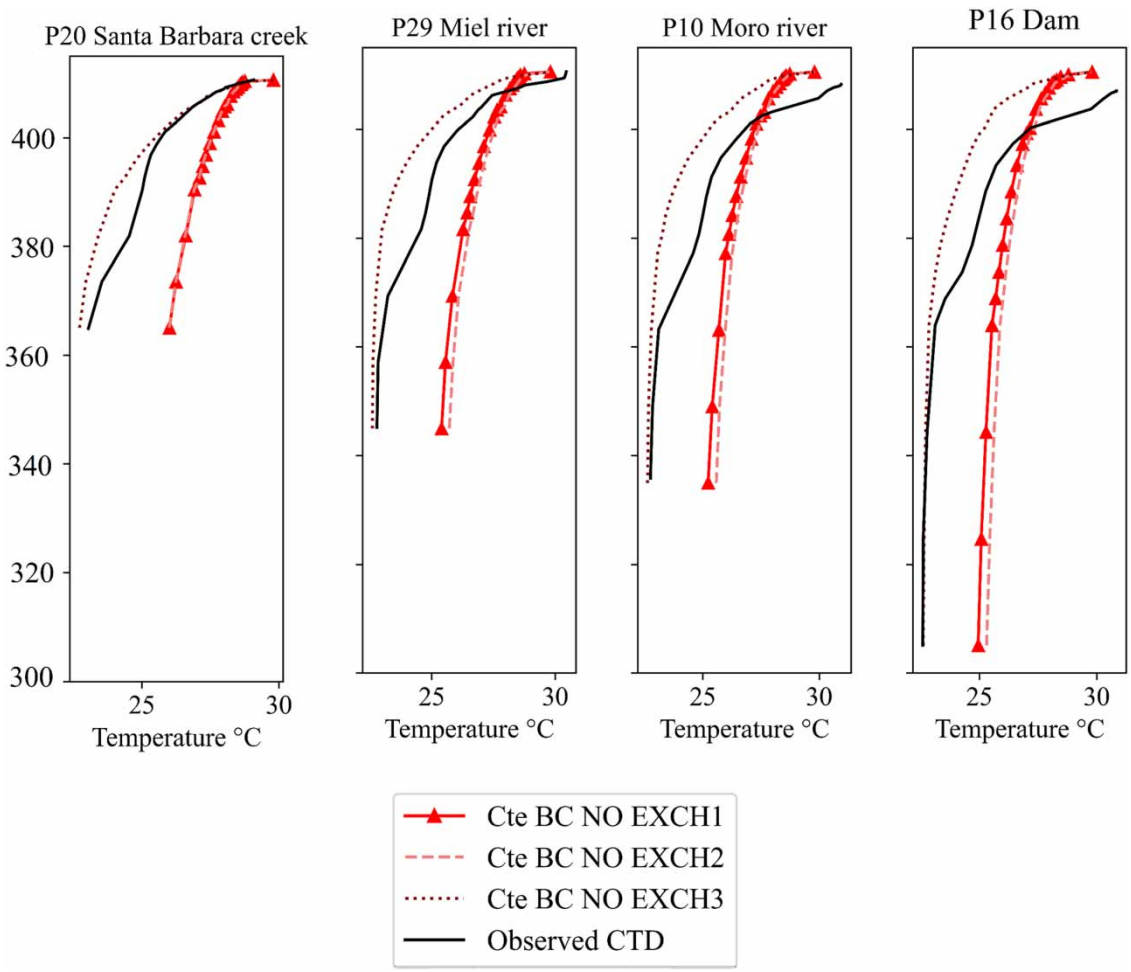

Figure 18 | Comparison between the vertical temperature profiles measured from the field and the simulated ones (17 August 2016).

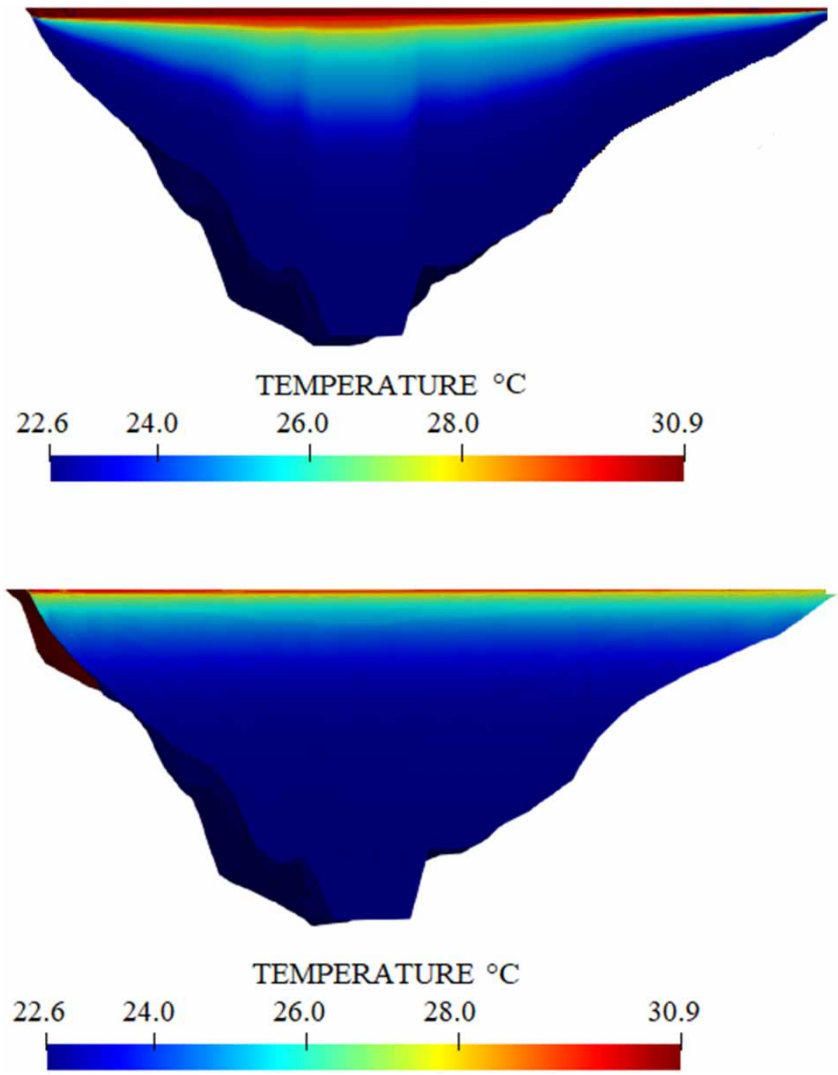

Figure 19 | The temperature distribution in a vertical plane near the dam (17 August 2016). Left: field data. Right: simulation result (case NO EXCH 3).

16 °C. During the study period, strong stratification was observed in the Amaní reservoir, with a temperature difference between the surface and the bottom reaching 8 °C according to both measurements and simulations. The water temperature difference between the surface and bottom was 4 °C in NO EXCH 1 and NO EXCH 2 along the reservoir in all simulated times, while its maximum of 7 °C was reached at NO EXCH 3. The thermal structure of simulation NO EXCH 3 exhibit fewer layers of stratification than actually observed.

4.2.2. Approach B: free surface boundary condition (Equation (12)) with meteorological parameters constant in time

Approach B explores what happens to the temperature profile for different values of the exchange coefficient A (Equation (13)) with constant meteorological forcing. The heat transfer coefficients or A value reported in (Williams 1963) for reservoirs present a range between $A \in [113, 378]$ W/m^2/°C. It was not possible to find more recent values reported in the studies. As shown in Table 2, this study varied b (involved in Equation (13)) in the range [0.001, 0.1]. The latter values correspond to a range of $A \in [15, 900]$ W/m^2/°C.

Table 3 shows the different values of the evaluated exchange coefficient A; however, only the results of the five most representative cases will be shown here. The influence of the simulated processes does not depend on the investigated location's depth but rather on the A value that shows a significant influence, with better results for higher values of A, as shown in the

Table 3 | Tested values of *A* exchange coefficient

b	*A* (W/m²/°C)
0.001	15
0.0025	30
0.0035	40
0.01	97
0.03	275
0.05	450
0.10	900

Figure 20. The cases with the best results are CAL2 and CAL3. The values of b are, respectively, 0.01 and 0.1, corresponding to $A = 97$ and 900 W/m^2/°C respectively. The case of CAL14 with a wind speed value of zero exhibited the highest error between 9.1 and 4.5% RE, RMSE between 2.4 and 1.2 °C, and MAE between 2.1 and 1.2 °C. Also, for these evaluated cases, the thermal diffusivity (k_T) does not show as significant an effect as in approach A. None of the cases presented a RE value of more than 10%. Furthermore, the RMSE and MAE values are below 5 °C.

Generally, the model has the most difficulty reproducing the behavior of the second layer and the bottom (Depths 2 and 4). The best results according to the metrics are discussed in detail in the next paragraph.

Observed and simulated water temperatures at the four depths during the analysis period are presented in Figure 21, showing the difference between the surface and bottom layers for measured and simulated water temperature. According to Figure 21, the model could represent the main observed patterns: (i) the mean value at hourly time scale on the first layer of the surface, which shows a value of 32 °C in CAL3, 28 °C for CAL2 and 26 °C for CAL1, for the period of analysis; (ii) cooling at the bottom of the reservoir revealed a 0.3 °C overestimation of CAL1 and CAL2, and 1 °C and more for CAL3. For the case of CAL3, there is a light tendency for a depth of 15 m and the bottom temperature to increase; (iii) the duration of the stratification period that never breaks in all cases, and is best represented for CAL3, with the exception of the bottom layer; (iv) Again, using approach B, it was not possible to reproduce the temperature oscillations in the upper layers, only the mean values. This is probably due to the meteorological forcing, constant in time.

Temporally, water temperature changes depend on the A air–water exchange coefficient. When A is lower, there is less exchange, and the water temperature experiences a drop, while when the A coefficient is higher, the water temperature rises. The case CAL2 is the one that is closest to the values observed at the free surface with an average of 28 °C; for the deeper layers, the A value that better represents the mean values is CAL 3.

Figure 22 shows the simulated and observed temperature profiles: vertical profiles at different points on the dam at a given time. It shows that the model can reasonably simulate the vertical stratification characteristics of the water temperature of the Amaní Reservoir, and case CAL3 is in good agreement with the observed water temperature structure of each analysis point. However, for these study cases, there are no mixing phenomena as identified for approach A, suggesting that it is necessary to determine the value of A that facilitates heat exchange to represent the vertical distribution of tropical reservoirs correctly.

The thermal structure along the reservoir near to dam is shown in Figure 23 for case CAL 3. As for approach A, it was not possible to reproduce the strongly stratified thermocline at depths of about 5 and 10 m with any simulations of approach B.

Vertically, strong stratification was observed in the reservoir for those scenarios, with the surface-bottom temperature difference reaching 8 °C in all the cases according to Figure 22. In agreement with other studies, stronger stratification has been reported in other deep reservoirs. Among them, the temperature difference between the surface and the bottom of the reservoir reaches 10 °C (70 m deep), and the maximum temperature difference of the other reservoirs even reaches 14 °C (200 m deep) (Plec *et al.* 2021). One main reason for these gradients is the depth of the Amaní reservoir with 120 m. By preventing the penetration of solar radiation and wind-driven eddies, large bodies of water like the Amaní reservoir impede heat transfer and make it difficult to achieve a homogeneous temperature. These variables, included in the A coefficient, represent radiation, air convection in contact with water, and latent heat. Its correct determination improves the simulation results compared with approach A from a temporal and vertical point of view.

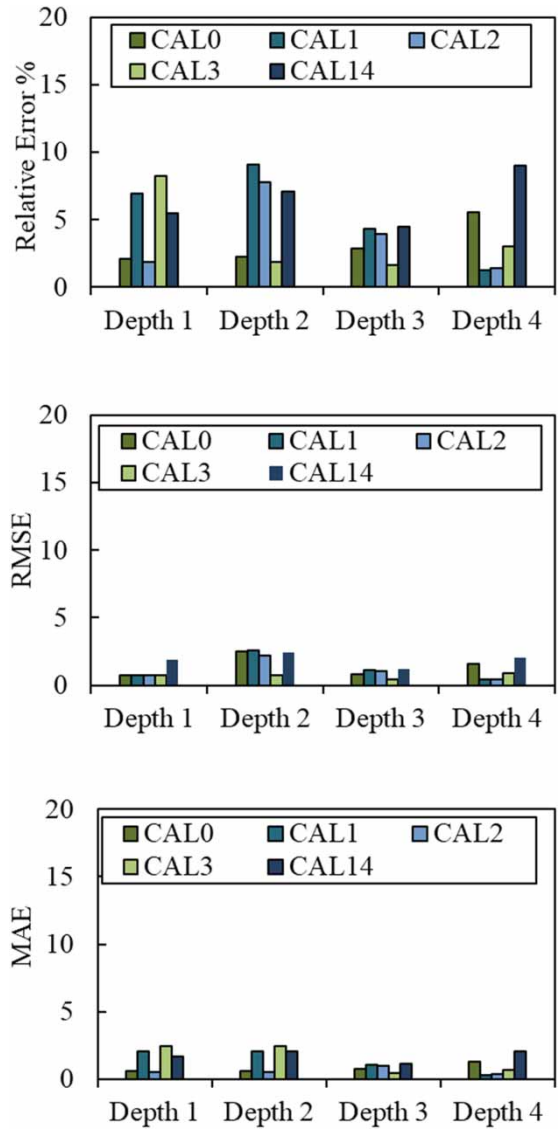

Figure 20 | Metrics for approach B, at different depths in the dam.

Longitudinally, the simulations of the temperature at the free surface drops at the entrance of the tributaries, and as the tributaries flowed toward the reservoir all the way down the dam, the simulated water surface temperature increases by 3.5 °C. Unfortunately, observed data do not provide any information on this phenomenon. The latter means that the heat transport in the reservoir is mainly due to advective transport, as was hypothesized, and in the first layer, it is due to the exchange of air–water and the atmospheric variables, mainly the exchange between air and water. Water is a poor conductor of heat, so thermal diffusion is slow in a reservoir. Therefore, the flow transfers energy with very high specific heat.

4.2.3 Approach C: free surface boundary condition (Equation (12) with meteorological parameters changing over time

The analysis of approach C explores what happens to the temperature profiles for different values of the exchange coefficient A when air temperature and wind change over time for a total of seven runs. The influence of the simulated processes does not depend on the investigated location's depth, but the A values as well as the oscillation of air temperature values show an influence of this location, with better results for lower values of A according Figure 24. The cases with the best results are Case CAL 1C with $A = 40\ \mathrm{W/m^2/°C}$, followed by CAL2 C with $A = 97\ \mathrm{W/m^2/°C}$. Case CAL 17

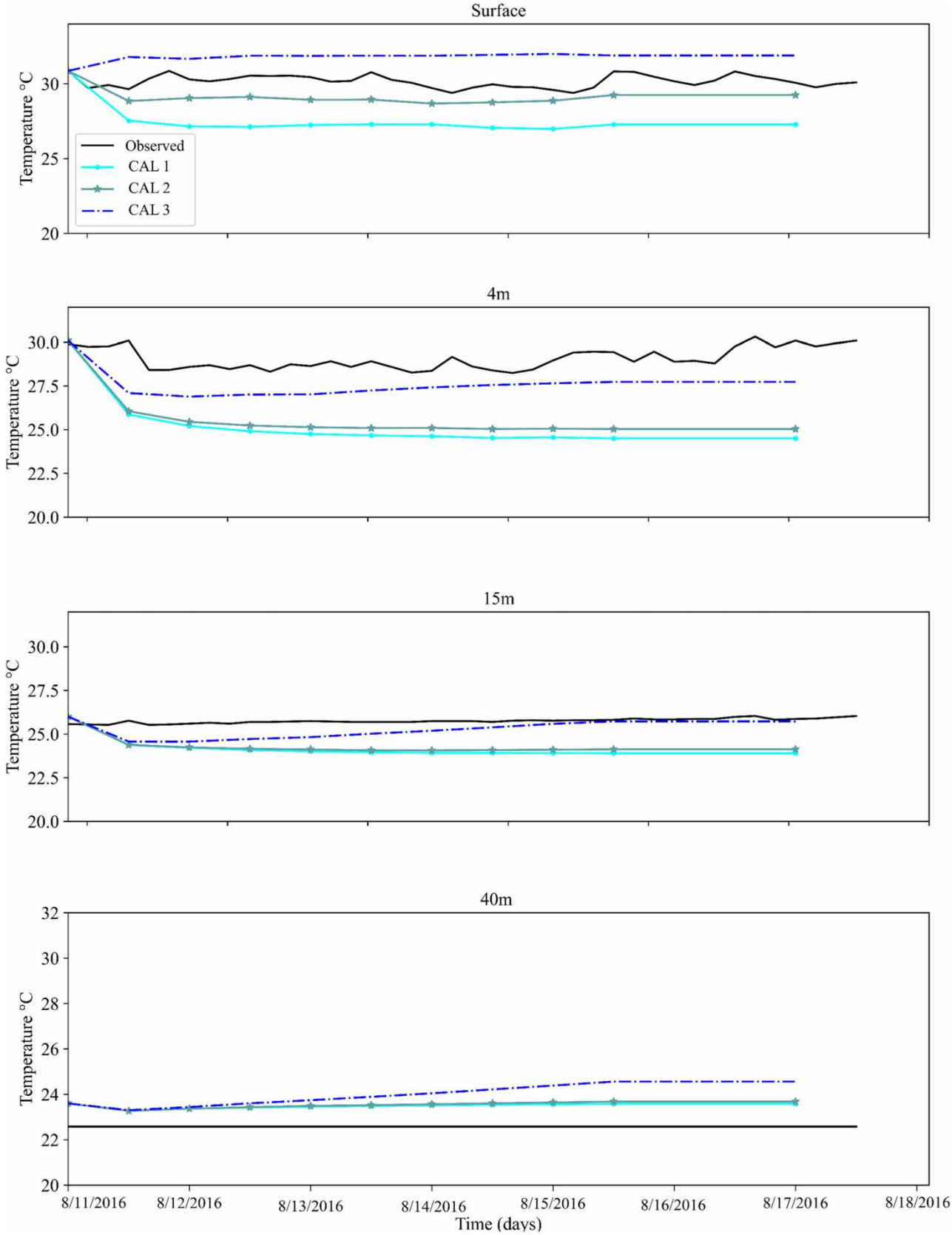

Figure 21 | Time variation of the observed and simulated temperatures at the dam with constant meteorological parameters.

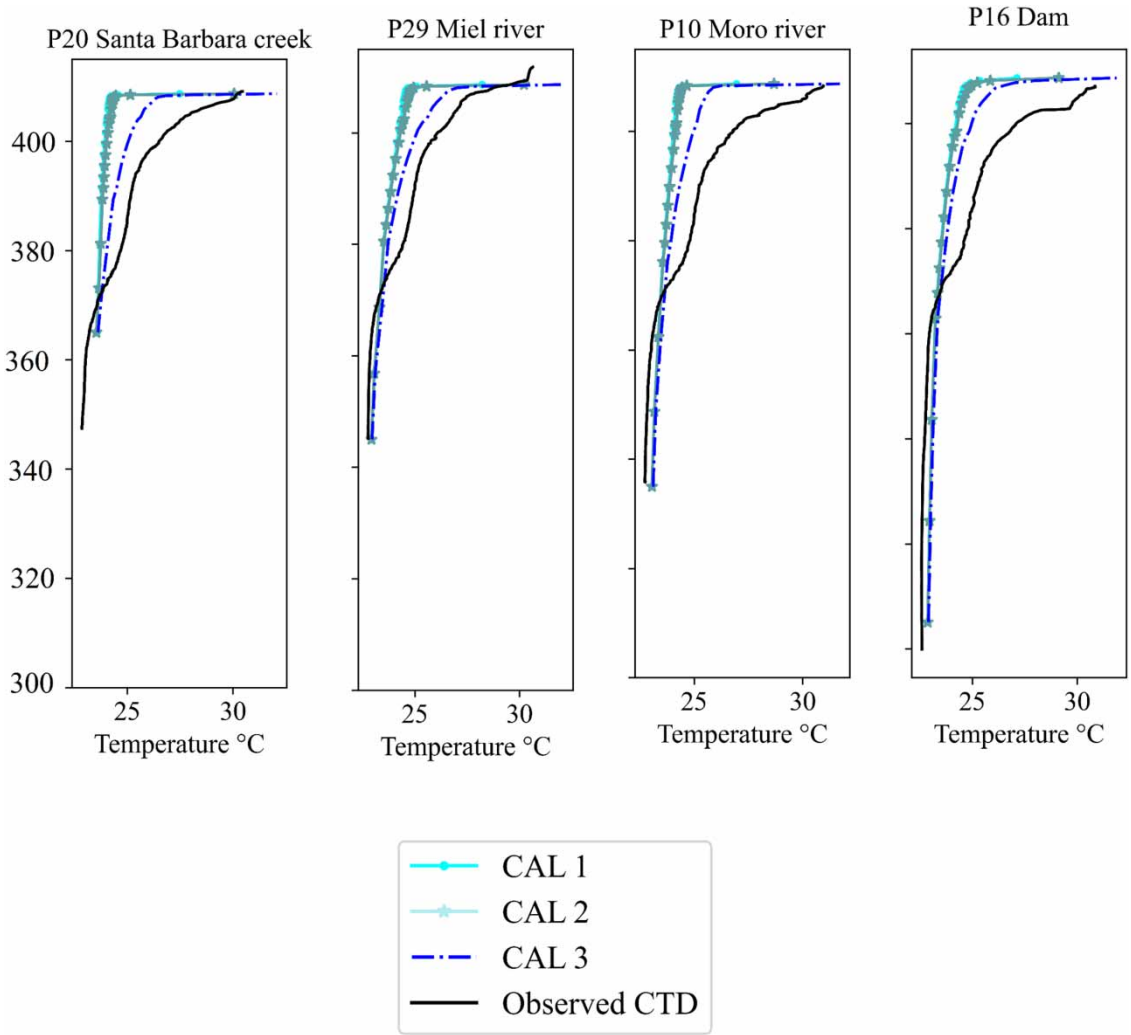

Figure 22 | Comparison between the vertical temperature profiles measured from the field and the simulated (17 August 2016).

was used to evaluate whether to further reducing the value of $A = 15$ W/m2/°C would improve the performance of the model, but it was not the case. In the case of CAL 15, since the initial conditions were taken from the last time step of CAL 3 and the diffusion coefficient was then set to zero, the results might have improved as the simulation time increased, but this did not happen, on the contrary.

CAL3C exhibited the highest errors with RE up to 16.3%, RMSE 5.0 °C, and MAE 3.7 °C. Furthermore, the A coefficient does not show as significant an effect as in approach B for these evaluation cases. All the simulations failed to reproduce the observed temperature at the free surface and the bottom (Depths 1 and 4). Those results are discussed in detail in the next paragraph. Observed and simulated water temperatures at the four depths during the analysis period are presented in Figure 25, showing the difference between the surface and bottom layers for measured and simulated water temperature.

The cases analyzed for approach C reproduces the observed temperature oscillations at the free surface and the 4 m layer, but they differ in the standard deviation temperatures. Data measured at the free surface exhibited temperature oscillations of up to 1.5 °C, compared to 2 °C for the studied CAL1C case, 3.5 °C for CAL2C, and 4.5 °C for CAL3C. Indeed, the amplitude of daily temperature variation decreases with A. Temporally, water temperature changes with air temperature. When the air temperature was lower than the water temperature, the water temperature experienced a drop, while when the air temperature was higher than the water temperature, the water temperature rose.

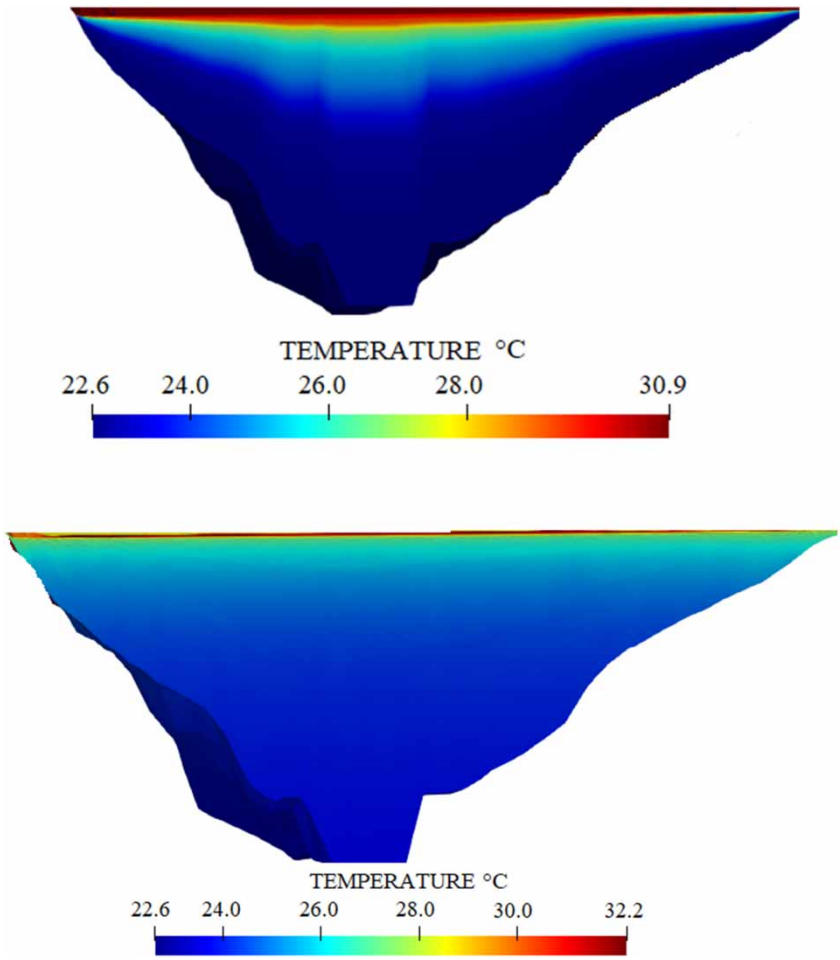

Figure 23 | The temperature distribution in a vertical plane near the dam on 17 August 2016. Left: field data. Right: simulation result (case CAL3).

According to Figure 25, the model could represent the main observed patterns: (i) the value at hourly time scale on the first layer of the surface, with a daily heat loss of about 4 °C for CAL1C, about 5 °C for CAL2C, and about 8 °C for CAL3C, for the period of analysis; (ii) at 4 m only CAL3C could reproduce water temperature oscillations but the average temperature is underestimated; (iii) cooling at the bottom of the reservoir revealed an overestimation of 0.4 °C for CAL1C and CAL2C and 0.7 °C for CAL3C.

Figure 26 shows the simulated and observed temperature profiles: vertical profiles at different points on the dam at a given time. It shows that the model can simulate a vertical stratification characteristic of the Amaní Reservoir's water temperature but does not agree with the observed water temperature structure at each analysis point. For these study cases, the mixing phenomena identified for approach A were not found here. Vertically, the water column along the reservoir is always stratified regardless of its position and depth (Figure 26 for points P20, P29, P10, and P16).

The thermal structure along the reservoir near the dam is shown in Figure 27 for case CAL1C. All simulations showed a maximum drop in water temperature of 8 °C at the free surface, but this was not observed. However, the case of CAL1C came closest to the data. For this approach during the period of study, only weak stratification was simulated in the thermal distribution, with the surface-bottom temperature difference reaching only 4 °C. In comparison, much stronger stratifications were simulated and observed at approach B.

In the case of approach C, the temperature oscillations at the free surface and at 4 m are simulated but the model still suffers from excessive heat losses, as the temperature of the layers below the air surface shows too significant daily decreases, which is not the case according to the observed data, as the air temperature shows oscillations of up to 14 °C. In contrast, the observed free surface temperature in the reservoir shows much smaller oscillations.

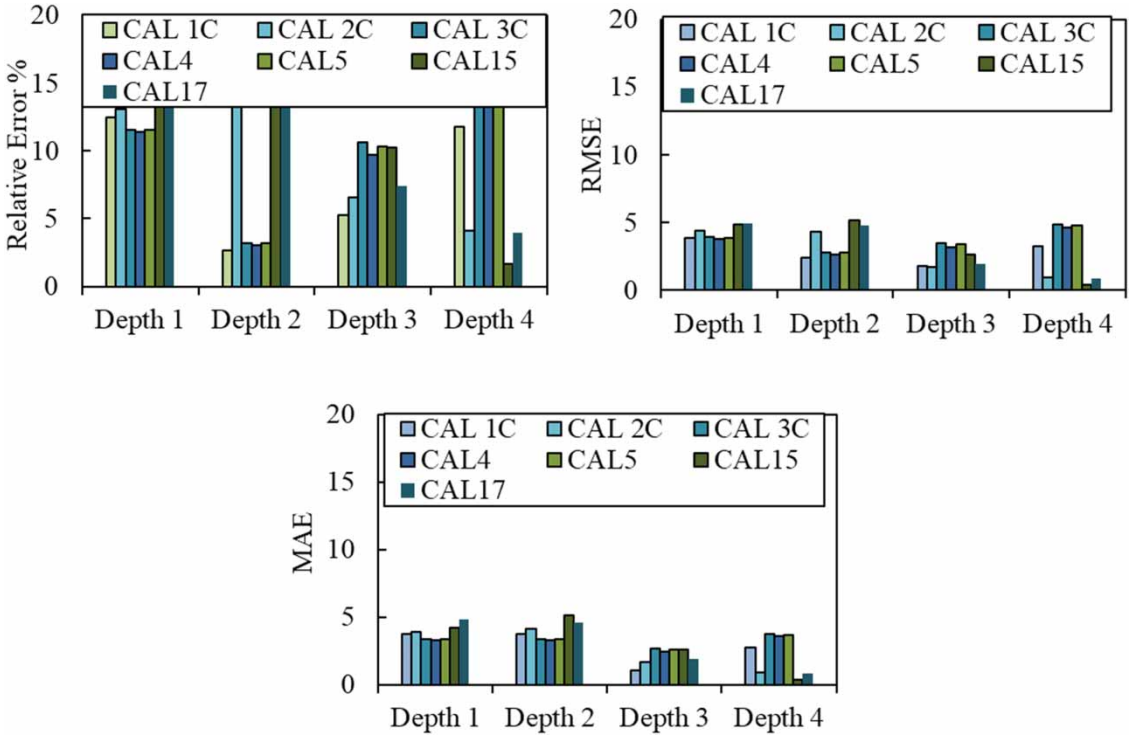

Figure 24 | Metrics for approach C, at different depths in the dam.

5. DISCUSSION

This study aims to understand the spatiotemporal exchange of tropical thermodynamics with the atmosphere. There are simulation tools that allow us to dig deeper into issues and knowledge, and potentially address scenarios such as climate change. However, when these tools are applied to an area as large as this case study, it often becomes a computational problem rather than a physical problem.

First, the use of a supercomputer includes decisions such as the number of processors and the desired computational time. This research used the OLYMPE supercomputer of CALMIP, supercomputing center which is providing resources and services for the entire scientific community of the Université Fédérale de Toulouse Midi-Pyrénées (UFTMiP). OLYMPE has a SEQUANA Cluster (ATOS-BULL) 1,365 Pflop/s, 374 computational nodes (36 cores/node), Intel® Skylake 6140 Processor at 2.3 Ghz 18-cores.

For hydrodynamics simulations, 36 cores showed real-time performance with a ratio of actual computational time to simulated time of 0.8–1. However, the thermal equations solution required more cores to achieve similar performance when solved simultaneously with hydrodynamics.

Different configurations were tested using 36, 64, 120, 180, 288, and 324 cores. Using 324 processors makes simulations very fast, e.g., it took 16–18 h to run 8 days of thermic simulations; however, increasing numbers of cores exhibit diminishing returns, and this study believes that using 180 cores (which takes approximately 24 h to run an 8-day simulation) provides the best balance between runtime and computing resources.

From the hydrodynamic perspective, several factors were analyzed, and it was found that specific parameters did not affect the thermal distribution, such as the use of hydrostatic pressure, horizontal turbulence models (Constant Viscosity, Smagorinsky, k–ω, and k–ε), coefficient for horizontal diffusion of velocities and the friction coefficient. While the number of vertical planes, Boussinesq approximation, the boundary conditions on the free surface, the vertical turbulence models (constant viscosity, mixing length, Smagorinsky, k–ω, and k–ε), and the value of the coefficient for vertical diffusion of velocities influenced the temperature distribution in the vertical direction. In several cases, the mixing-length turbulence model results in faster mixing in the vertical direction than the observed thermal profile data, while constant viscosity best represents the thermal distribution in the vertical direction.

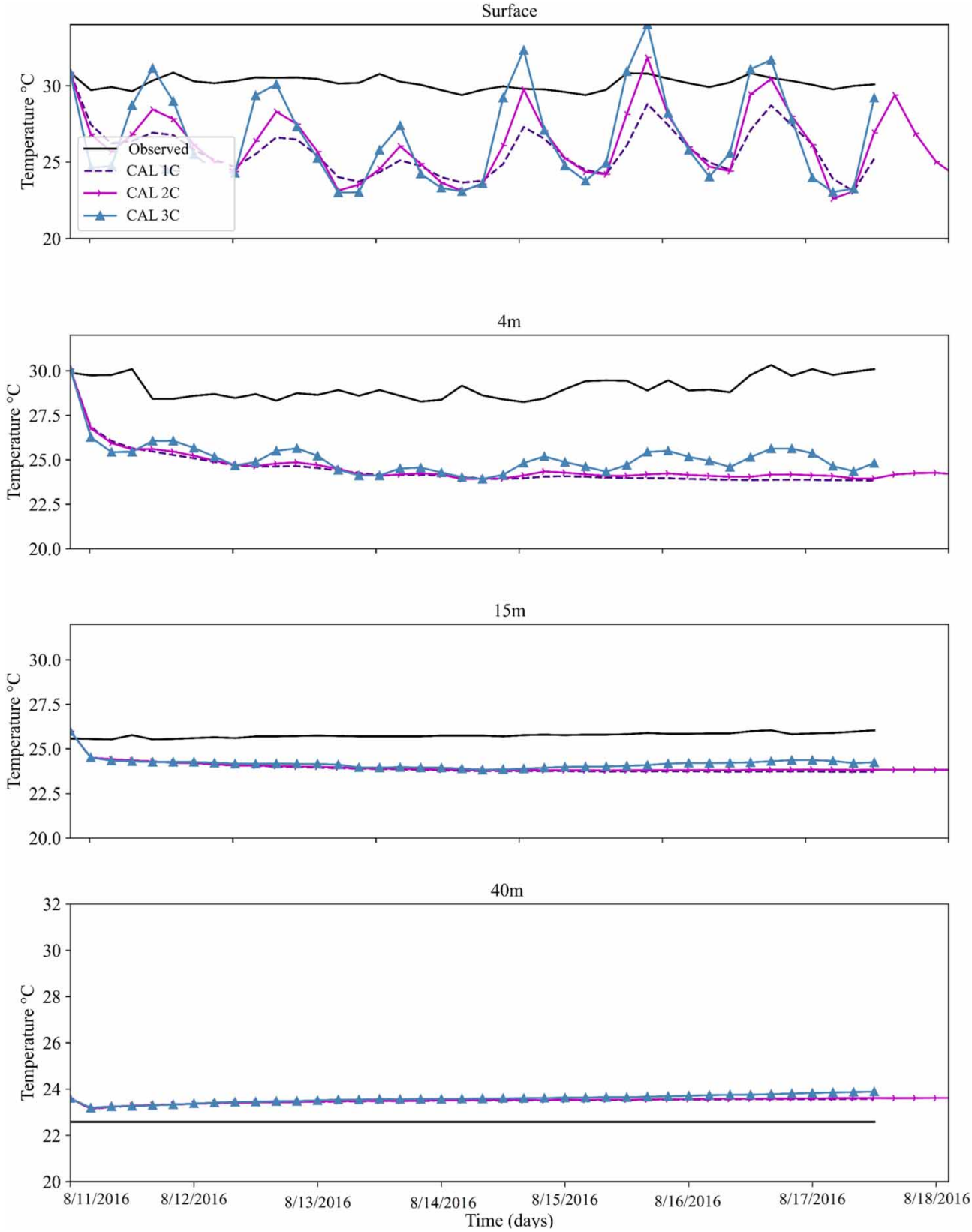

Figure 25 | Time variation of the observed and simulated temperatures at the dam with exchange with the atmosphere, with meteorological parameters changing.

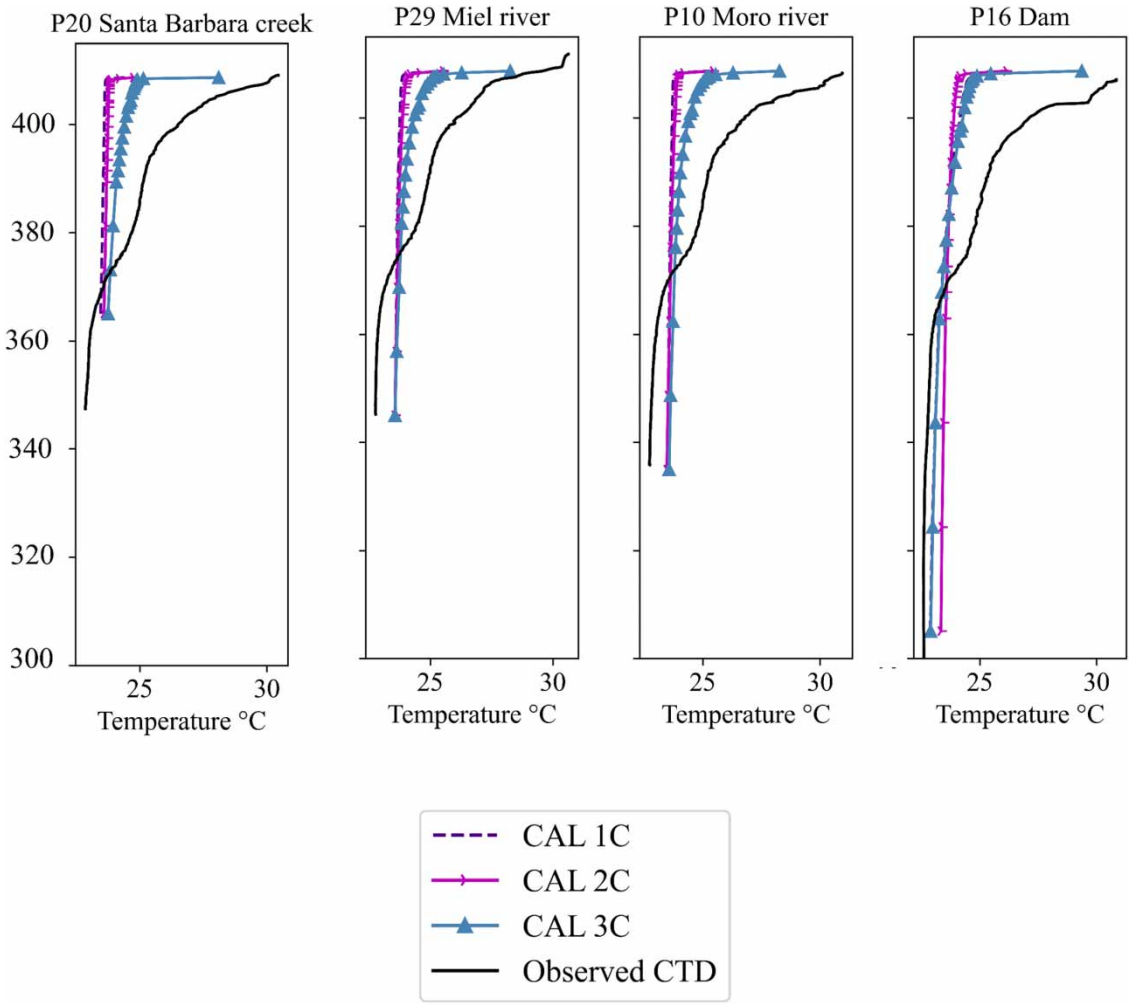

Figure 26 | Comparison between the vertical temperature profiles measured from the field and the simulated (17 August).

Regarding the thermal dynamics, this research found that the structure of the solution was very sensitive to the choice of an advection scheme. Seven methods for linear advection treatment (1) Method of characteristics, (2) Streamline Upwind Petrov Galerkin (semi-implicit), (3) Explicit finite volumes, (4) Explicit scheme + MURD (MURD) N scheme, (5) Explicit scheme + MURD PSI (TELEMAC 2020) (Positive Streamwise Invariant) scheme, (6) Explicit Leo Postma scheme for tidal flats, (7) Explicit scheme + MURD N scheme were used to analyze the behavior of the solution. Only the most relevant simulations were shown here for the sake of conciseness. Compared to other schemes, it was found that the MURD N scheme produces fewer numerical oscillations, less diffusion perpendicular to flow and thermodynamics, and is less computationally expensive. The scheme is also characterized by being conditional on a Courant number less than 1, satisfying the stability criterion.

The exchange process with the atmosphere is an essential and well-studied physical process. The tools used for its mathematical representation are still very limited, e.g., in the first layer of water temperature, the exchange between air and water also explains the behavior. The observations indicate that the external heat flux, which is determined by meteorological and inflow conditions, is insufficient to modify the nearly stratified state of the tropical reservoir. Many formulae in the studies can be used to compute this term (Equation (10)) but selecting an appropriate one is debatable. Generally, the net heat flux is calculated based on the water temperature and various meteorological data, primarily based on air temperature, air humidity, air pressure, measured shortwave solar radiation, and wind speed (although many others may be taken into account). An estimate of the net heat flux at the water–air interface turns out to be a challenge, especially when it comes to 3D modeling.

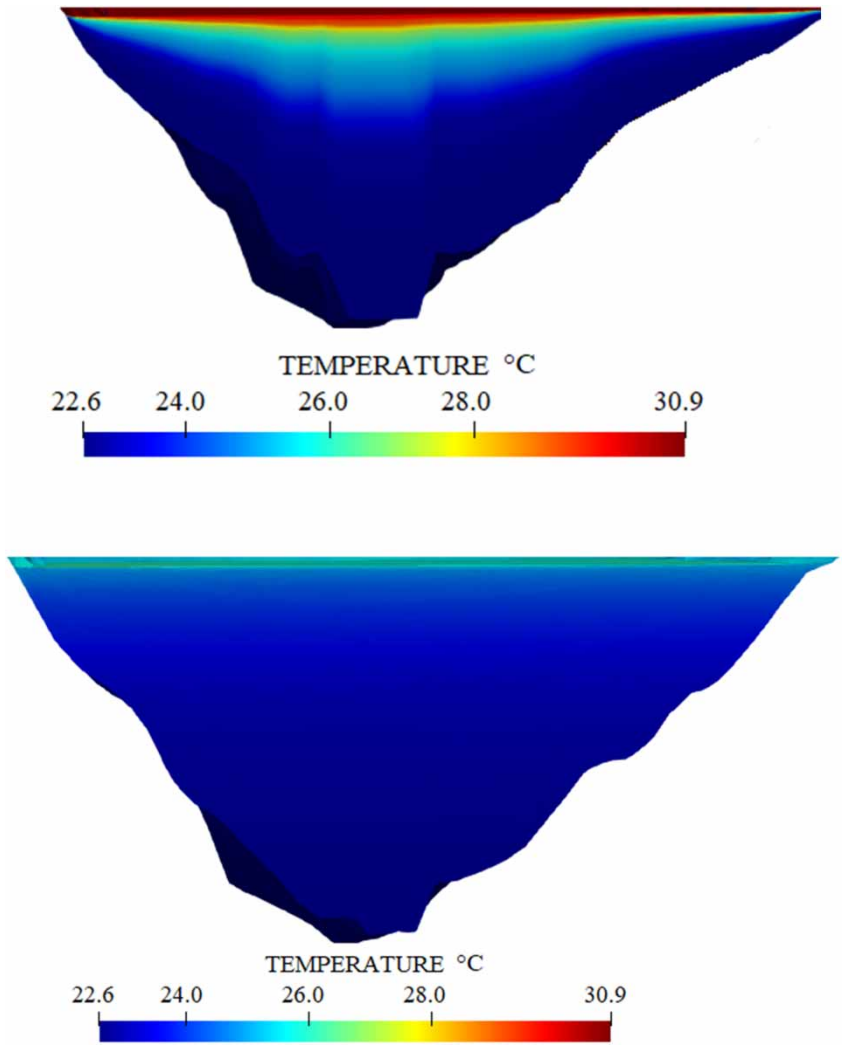

Figure 27 | The temperature distribution in a vertical plane near the dam on 17 August 2016. Left: field data. Right: simulation result (case CAL 1C).

The first problem concerns obtaining the necessary input data for the analyzed site. Intuitively, the nearest meteorological station is the best source for meteorological data. Unfortunately, in many cases, the nearest station does not provide all the necessary data or is still too far from the considered study zone. Another problem is the differences in data obtained from the neighboring stations. Even in conducive situations when the necessary meteorological data are available near the reservoir, there are still uncertainties related to the station's location, for which conditions such as shading or wind speed are often considerably different from those at the reservoir.

The problem is widely discussed in the work (Benyahya *et al.* 2010). Moreover, some measured quantities may vary along the reservoir (or even across the reservoir width). Finally, very different values of net heat flux may be obtained. Williams (1963), for example, measured the heat fluxes for several reservoirs in different conditions. The results showed that the final sum of heat fluxes measured ranged between 113 and 378 $W/m^2/°C$. In this case shows that A coefficient exchange value depends on the meteorological conditions, if they are constant over time or changing, and this research found the approximate values that can be used in tropical environment reservoirs.

Additionally, each term in Equation (12) is sensitive to several factors, and the chosen computation method, i.e., different formulae, may lead to varying results since they often depend on not well-defined parameters, factors, or coefficients site-specific. Moreover, in the 'competition' for the best formula, increasingly 'more accurate' formulae take into account more and more factors and thus require more and more input data, which, again in practical applications, are rarely available or highly uncertain.

6. CONCLUSION

In this work, different modeling assumptions for tropical reservoir temperature and air–water exchange are analyzed based on observations. This study evaluated the performance of various hypothesis in resolving hydrodynamic, thermal, and energetic processes, including the effect of hydroclimatological forcings such as air temperature, wind, and the internal mixing process (turbulence), and different boundary conditions in the free surface. The following conclusions can be drawn:

Reservoir water temperature is affected by heat exchange between the water and the atmosphere. This exchange is evident in the upper layer (O (<10 m)), and it is this dynamic in the first layer governs the distribution within the water body in areas where there is no advective flow from tributaries, which for the reservoir analyzed is on the order of 80%.

It was observed that the reservoir is permanently stratified and, unlike other reservoirs in the temperate zone, is not significantly affected by meteorological conditions outside the water body. This means that the thermal dynamics inside the reservoir remain very constant. In this work, numerical methods are used as a tool to study exchange. This research finds that a good definition of the boundary conditions at the water-free surface is crucial for a correct representation of the thermodynamics inside the water body.

The hydrodynamic TELEMAC-3D model has been satisfactorily calibrated using one month of daily water level observations at one point in the reservoir. Sensitivity analyses highlighted the importance of vertical turbulence models and vertical diffusion coefficient for a correct representation of the observed behavior.

Overall, reservoir water temperature is strongly influenced by heat exchange between water and the atmosphere. Accurate modeling of such phenomena is thus necessary. Three different approaches have been tested to study the impact of air–water exchanges at the free surface: a constant water temperature without exchange with the atmosphere (approach A), meteorological forcing with atmospheric parameters constants in time (approach B), meteorological forcing with atmospheric parameters varying in time (approach C).

Not considering the exchange process at the free surface can produce a good performance in the first layers of the reservoir (approach A). However, it may lead to overestimating the measured temperature in the deepest layers due to non-observed mixing processes. Moreover, it does not allow to simulate daily temperature oscillations.

Approach B with constant values of air temperature and wind, is the one that best represents the thermal stratification in terms of thermal distribution in the reservoir; however, there are excessive heat losses, which do not occur in reality. To better control these losses, Mesquita *et al.* (2020) recommend explicitly simulating evaporation in the reservoir.

Although approach C is the only approximation that shows hourly fluctuations in the temperature of the first layer of the reservoir, these fluctuations are larger than the observed ones. Simulation results show oscillations between 2 and 4.5 °C, whereas observed variations range between 1 and 2 °C. This may be due to the fact that the reservoir is located in a relatively sheltered canyon, as mentioned by Plec *et al.* (2021).

The results show that the parameter that mainly influences the thermal exchange model, thus improving the numerical reproduction of the thermal stratification processes, is the exchange coefficient A. A represent processes such as radiation, air convection in contact with water, and latent heat. Its correct determination improves the simulation results. According to the results of this study, when taking into account the exchange process between the water and the atmosphere under different forcings of the meteorological variables, a range of variation of $A\in$ [100, 900] W/m2/°C is best when the air temperature remains constant over time and lower values of $A\in$ [30, 40] W/m2/°C are best when weather conditions vary over time.

Although some uncertainties are present in the current numerical study about the A exchange coefficient tested in the simulations, the results are in a satisfactory agreement to data, especially considering the complexity of the studied phenomenon, as well as the equally complex dynamics of the various processes' interactions involved in its numerical simulation. In particular, regarding the water temperature at different depths, the following convergence results are observed: approach A maximum deviation from data reaching 3 °C, approach B maximum deviation from data reaching 4 °C, and approach C maximum deviation from data reaching 8 °C.

In conclusion, it can be stated that if site conditions and air–water temperature differences are known, A coefficient can be used as an approximate method of estimating the rate of exchange of natural water surfaces in a reservoir on an hourly basis during every period in the year.

Overall, we showed the potential and limitations of present three-dimensional hydraulic models in predicting the vertical distribution of temperature in tropical reservoirs. Future works will require rethinking the exchange formulae for the tropical context including evaporation, as the existing ones are not able to reproduce the variations in the water column of the reservoirs.

ACKNOWLEDGEMENTS

The authors would like to thank the Institut de Mécanique des Fluides de Toulouse, especially Maxime Pigou from the code and numerical simulations service and University of Medellin for providing us with the resources and support we needed to complete this project. This work was granted access to the HPC resources of CALMIP supercomputing center under the allocation 22AP22035.

AUTHOR CONTRIBUTIONS

J.A. was involved in conceptualization, methodology, software, investigation, writing – original draft. H.R. was involved in validation, resources, writing – review & editing, supervision. L.C. was involved in validation, resources, writing – review & editing, supervision. T.B. was involved in validation, resources, writing – review & editing, supervision. J.E. was involved in conceptualization and supervision. L.J.M. was involved in data curation and supervision.

DATA AVAILABILITY STATEMENT

All relevant data are included in the paper or its Supplementary Information.

CONFLICT OF INTEREST

The authors declare there is no conflict.

REFERENCES

Agostinho, A. A., Pelicice, F. M. & Gomes, L. C. 2008 Dams and the fish fauna of the Neotropical region: Impacts and management related to diversity and fisheries. *Brazilian Journal of Biology* **68** (4 suppl), 1119–1132. https://doi.org/10.1590/S1519-69842008000500019.

Alzate-Gómez, J.-A., Aguirre-Duran, C., Escobar-Vargas, J. A., Montoya-Jaramillo, L.-J. & Piedrahita-Escobar, C.-C. 2023 On the spatial-temporal behavior, and on the relationship between water quality and hydrometeorological information to predict dissolved oxygen in tropical reservoirs. Case study: La Miel, Hydropower Dam. *Air, Soil and Water Research* **16**, 1–15. https://doi.org/10.1177/11786221221150189.

Amorim, C. A., Dantas, Ê. W. & Moura, A. d. N. 2020 Modeling cyanobacterial blooms in tropical reservoirs: The role of physicochemical variables and trophic interactions. *Science of The Total Environment* **744**, 140659. https://doi.org/10.1016/J.SCITOTENV.2020.140659.

Amorim, L. F., Martins, J. R. S., Nogueira, F. F., Silva, F. P., Duarte, B. P. S., Magalhães, A. A. B. & Vinçon-Leite, B. 2021 Hydrodynamic and ecological 3D modeling in tropical lakes. *SN Applied Sciences* **3** (4), 444. https://doi.org/10.1007/s42452-021-04272-6.

Angelotti, N., Vinçon-Leite, B. & Carmigniani, R. 2021 *Hydrodynamic Modelling for Early Warning of Sanitary Risks in Open Swimming Waters*. In: Breugem, W. A., Frederickx, L., Koutrouveli, T., Chu, K., Kulkarni, R. & Decrop, B. (eds.): Proceedings of the papers submitted to the 2020 TELEMAC-MASCARET User Conference October 2021. Antwerp: International Marine and Dredging Consultants (IMDC). S. 175–180. Available from: https://hdl.handle.net/20.500.11970/108309.

Azadi, F., Ashofteh, P.-S. & Loáiciga, H. A. 2019 Reservoir water-quality projections under climate-change conditions. *Water Resources Management* **33** (1), 401–421. https://doi.org/10.1007/s11269-018-2109-z.

Basso, M., Mateus, M., Ramos, T. B. & Vieira, D. C. S. 2021 Potential post-fire impacts on a water supply reservoir: An integrated watershed-Reservoir approach. *Frontiers in Environmental Science* **9**. https://doi.org/10.3389/fenvs.2021.684703.

Bedri, Z., Bruen, M., Dowley, A. & Masterson, B. 2013 Environmental consequences of a power plant shut-down: A three-dimensional water quality model of Dublin Bay. *Marine Pollution Bulletin* **71** (1–2), 117–128. https://doi.org/10.1016/j.marpolbul.2013.03.025.

Benyahya L., Caissie D., El-Jabi N. & Satish M. G. 2010 Comparison of microclimate vs. remote meteorological data and results applied to a water temperature model (Miramichi River, Canada). *Journal of Hydrology* **380**, 247–259.

Chai, T. & Draxler, R. R. 2014 Root mean square error (RMSE) or mean absolute error (MAE)? – Arguments against avoiding RMSE in the literature. *Geoscientific Model Development* **7** (3), 1247–1250. https://doi.org/10.5194/gmd-7-1247-2014.

Chen, Y. 2020 *Numerical Study of the Hydrodynamics of Fangar Bay by Using Unstructured Meshes – Analysis of Diffusion by Using Salinity as A Tracer with the TELEMAC 3D Model*.

Chuo, M., Ma, J., Liu, D. & Yang, Z. 2019 Effects of the impounding process during the flood season on algal blooms in Xiangxi Bay in the Three Gorges Reservoir, China. *Ecological Modelling* **392**, 236–249. https://doi.org/10.1016/j.ecolmodel.2018.11.017.

Cooper, A. J. & Spearman, J. 2017 *Validation of A TELEMAC-3D Model of a Seamount*, Vol. 17. Available from: www.opentelemac.org

Costi, J., Forster, A., Marques, W. C., Duarte, R. F. & Arigony-Neto, J. 2019 Application of the TELEMAC-3D to simulate flooding and hydrodynamic patterns of Southern Brazilian wetlands. In *XXVIth TELEMAC-MASCARET User Conference*.

Crowe, S. A., O'Neill, A. H., Katsev, S., Hehanussa, P., Haffner, G. D., Sundby, B., Mucci, A. & Fowle, D. A. 2008 The biogeochemistry of tropical lakes: A case study from Lake Matano, Indonesia. *Limnology and Oceanography* **53** (1), 319–331. https://doi.org/10.4319/lo.2008.53.1.0319.

Curtarelli, M. P., Alcântara, E. H., Rennó, C. D. & Stech, J. L. 2013 Modeling the effects of cold front passages on the heat fluxes and thermal structure of a tropical hydroelectric reservoir. *Hydrology & Earth System Sciences Discussions* **10**, 8467–8850.

da Silva, M. C., de Paula Kirinus, E., Bendô, A. R. R., Marques, W. C., Vargas, M. M., Leite, L. R., Junior, O. O. M. & Pertille, J. 2021 Dynamic modeling of effluent dispersion on Mangueira bay – Patos Lagoon (Brazil). *Regional Studies in Marine Science* **41**. https://doi.org/10.1016/j.rsma.2020.101544.

Duarte, B., Amorim, L., Martins, J. R. & Bernardino, J. C. 2021 Comparison of 1D and 3D hydrodynamic models on the assessement of climate change scenarios impact over a small tropical lake. In *EGU General Assembly 2021*.

Elçi, Ş. 2008 Effects of thermal stratification and mixing on reservoir water quality. *Limnology* **9** (2), 135–142. https://doi.org/10.1007/s10201-008-0240-x.

Gaeta, M. G., Samaras, A., Archetti, R. & Lamberti, A. 2015 *Numerical Investigation of Thermal Discharge to Coastal Areas Using TELEMAC-3D: A Case Study for South Italy*. Available from: https://www.researchgate.net/publication/279758154

Gaeta, M. G., Samaras, A. G. & Archetti, R. 2020 Numerical investigation of thermal discharge to coastal areas: A case study in South Italy. *Environmental Modelling & Software* **124**, 104596. https://doi.org/10.1016/j.envsoft.2019.104596.

Gassman, W., M, P., Reyes, R., Green, C. H. & Arnold, J. G. 2007 The soil and water assessment tool: Historical development, applications, and future research directions. *Transactions of the ASABE* **50** (4), 1211–1250. https://doi.org/10.13031/2013.23637.

Gooseff, M. N., Strzepek, K. & Chapra, S. C. 2005 Modeling the potential effects of climate change on water temperature downstream of a shallow reservoir, lower Madison river, MT. *Climatic Change* **68** (3), 331–353. https://doi.org/10.1007/s10584-005-9076-0.

Goudsmit, G.-H., Burchard, H., Peeters, F. & Wüest, A. 2002 Application of k-ε turbulence models to enclosed basins: The role of internal seiches. *Journal of Geophysical Research: Oceans* **107** (C12), 23-1–23–13. https://doi.org/10.1029/2001JC000954.

Halini Baharim, N., Ismail, R. & Hanif Omar, M. 2011 Effects of thermal stratification on the concentration of iron and manganese in a tropical water supply reservoir. *Sains Malaysiana* **40** (8), 821–825.

Hervouet, J. 2007 *Hydrodynamics of Free Surface Flows*. Wiley. https://doi.org/10.1002/9780470319628.

Hinkelmann, R. 2005 *Efficient Numerical Methods and Information-Processing Techniques for Modeling Hydro- and Environmental Systems*, Vol. 21. Springer-Verlag. https://doi.org/10.1007/3-540-32379-1.

Huszar, V. L. M., Caraco, N. F., Roland, F. & Cole, J. 2006 Nutrient–chlorophyll relationships in tropical–subtropical lakes: Do temperate models fit? *Biogeochemistry* **79** (1–2), 239–250. https://doi.org/10.1007/s10533-006-9007-9.

Jiang, B., Wang, F. & Ni, G. 2018 Heating impact of a tropical reservoir on downstream water temperature: A case study of the Jinghong Dam on the Lancang River. *Water* **10** (7), 951. https://doi.org/10.3390/w10070951.

Justin-Brochet, E., Pham, C.-T. & Vidal-Hurtado, J. 2021 *Recent Improvements for the Berre Lagoon Modelling with TELEMAC-3D*. In: Breugem, W. A., Frederickx, L., Koutrouveli, T., Chu, K., Kulkarni, R. & Decrop, B. (eds.): Proceedings of the papers submitted to the 2020 TELEMAC-MASCARET User Conference October 2021. Antwerp: International Marine and Dredging Consultants (IMDC). S. 26–33. Available from: https://hdl.handle.net/20.500.11970/108311.

Katsev, S., Crowe, S. A., Mucci, A., Sundby, B., Nomosatryo, S., Haffner, G. D. & Fowle, D. A. 2010 Mixing and its effects on biogeochemistry in the persistently stratified, deep, tropical Lake Matano, Indonesia. *Limnology and Oceanography* **55** (2), 763–776. https://doi.org/10.4319/lo.2010.55.2.0763.

Killingtveit, Å. 2019 Hydropower. In: *Managing Global Warming*. Elsevier, pp. 265–315. https://doi.org/10.1016/B978-0-12-814104-5.00008-9.

Kopmann, R. & Markofsky, M. 2000 Three-dimensional water quality modelling with TELEMAC-3D. *Hydrological Processes* **14** (13), 2279–2292. https://doi.org/10.1002/1099-1085(200009)14:13<2279::AID-HYP28 > 3.0.CO;2-7.

Kuriqi, A., Pinheiro, A. N., Sordo-Ward, A., Bejarano, M. D. & Garrote, L. 2021 Ecological impacts of run-of-river hydropower plants – Current status and future prospects on the brink of energy transition. *Renewable and Sustainable Energy Reviews* **142**, 110833.

Labaj, A. L., Michelutti, N. & Smol, J. P. 2018 Annual stratification patterns in tropical mountain lakes reflect altered thermal regimes in response to climate change. *Fundamental and Applied Limnology* **191** (4), 267–275. https://doi.org/10.1127/fal/2018/1151.

Laval, B. E., Imberger, J. & Findikakis, A. N. 2005 Dynamics of a large tropical lake: Lake Maracaibo. *Aquatic Sciences* **67** (3), 337–349. https://doi.org/10.1007/s00027-005-0778-1.

Lewis, W. M. 1996 Tropical lakes: How latitude makes a difference. In: Schiemer F. & K. Boland, T. Eds., Perspectives in Tropical Limnology, SPB Academic Publishing, Amsterdam, 1996, pp. 43–64.

Ligier, P.-L. & Okumura, N. 2019 Three-dimensional hydrodynamic modelling in a bay of the Lake Mälaren to assess environmental impacts from a cooling and heating power plant production. In *XXVIth TELEMAC-MASCARET User Conference*.

Lindenschmidt, K.-E., Carr, M. K., Sadeghian, A. & Morales-Marin, L. 2019 CE-QUAL-W2 model of dam outflow elevation impact on temperature, dissolved oxygen and nutrients in a reservoir. *Scientific Data* **6** (1), 312. https://doi.org/10.1038/s41597-019-0316-y.

Lindim, C., Pinho, J. L. & Vieira, J. M. P. 2011 Analysis of spatial and temporal patterns in a large reservoir using water quality and hydrodynamic modeling. *Ecological Modelling* **222** (14), 2485–2494. https://doi.org/10.1016/j.ecolmodel.2010.07.019.

Lisboa, P. V. & Fernandes, E. H. 2015 Anthropogenic influence on the sedimentary dynamics of a sand spit bar, Patos Lagoon Estuary, RS, Brazil. *Revista de Gestão Costeira Integrada*, 35–46. https://doi.org/10.5894/rgci541.

Marín-Ramírez, A., Gómez-Giraldo, A. & Román-Botero, R. 2020 Seasonal variability of advective and atmospheric heat fluxes and mean temperature in a tropical Andean reservoir. *Revista de La Academia Colombiana de Ciencias Exactas, Fisicas y Naturales* **44** (171), 360–375. https://doi.org/10.18257/raccefyn.1081.

Matta, E., Selge, F., Gunkel, G. & Hinkelmann, R. 2017 Three-dimensional modeling of wind- and temperature-induced flows in the Icó-Mandantes Bay, Itaparica Reservoir, NE Brazil. *Water (Switzerland)* **9** (10), 772. https://doi.org/10.3390/w9100772.

Merkel, U. H. 2019 Thermal Stratification in Small Lakes with TELEMAC-3D: Showcase 'Lake Monsterloch'. In *XXVIth TELEMAC-MASCARET User Conference*. https://doi.org/10.5281/zenodo.3611576.

Mesquita, J. B. d. F., Lima Neto, I. E., Raabe, A. & de Araújo, J. C. 2020 The influence of hydroclimatic conditions and water quality on evaporation rates of a tropical lake. *Journal of Hydrology* **590**, 125456. https://doi.org/10.1016/J.JHYDROL.2020.125456.

Moloney, V., Karunarathna, H., Murray, T., Rutt, I., Everett, A. & Reeve, D. 2016 Investigation of wind and tidal forcing on stratified flows in Greenland fjords with TELEMAC-3D. *European Journal of Computational Mechanics* **25** (3), 249–272. https://doi.org/10.1080/17797179.2016.1191121.

Pajares, S., Merino-Ibarra, M., Macek, M. & Alcocer, J. 2017 Vertical and seasonal distribution of picoplankton and functional nitrogen genes in a high-altitude warm-monomictic tropical lake. *Freshwater Biology* **62** (7), 1180–1193. https://doi.org/10.1111/fwb.12935.

Piccioni, F., Vinçon-Leite, B., Le, M.-H. & Casenave, C. 2021 *Aquatic Ecological Modelling with TELEMAC3D: Performance of the Ecological Library AED2 in a Natural Ecosystem*. In: Breugem, W. A., Frederickx, L., Koutrouveli, T., Chu, K., Kulkarni, R. & Decrop, B. (eds.): Proceedings of the papers submitted to the 2020 TELEMAC-MASCARET User Conference October 2021. Antwerp: International Marine and Dredging Consultants (IMDC). S. 168–174. Available from: https://hdl.handle.net/20.500.11970/108308.

Pimenta, A. M., Albertoni, E. F. & Palma-Silva, C. 2012 Characterization of water quality in a small hydropower plant reservoir in southern Brazil. *Lakes & Reservoirs: Science, Policy and Management for Sustainable Use* **17** (4), 243–251. https://doi.org/10.1111/lre.12007.

Plec, D. F., Silva, T. F. d. G., Vinçon-Leite, B. & Nascimento, N. 2021 Thermal functioning of a tropical reservoir assessed through three-dimensional modelling and high-frequency monitoring. *RBRH* **26**. https://doi.org/10.1590/2318-0331.262120200150.

Politano, M., Haque, M. M. & Weber, L. J. 2008 A numerical study of the temperature dynamics at McNary Dam. *Ecological Modelling* **212** (3–4), 408–421. https://doi.org/10.1016/J.ECOLMODEL.2007.10.040.

Rajabi, M. M., Ataie-Ashtiani, B. & Simmons, C. T. 2015 Polynomial chaos expansions for uncertainty propagation and moment independent sensitivity analysis of seawater intrusion simulations. *Journal of Hydrology* **520**, 101–122. https://doi.org/10.1016/J.JHYDROL.2014.11.020.

Rangel, L. M., Silva, L. H. S., Arcifa, M. S. & Perticarrari, A. 2009 Driving forces of the diel distribution of phytoplankton functional groups in a shallow tropical lake (Lake Monte Alegre, Southeast Brazil). *Brazilian Journal of Biology* **69** (1), 75–85. https://doi.org/10.1590/S1519-69842009000100009.

Rueda, F., Moreno-Ostos, E. & Armengol, J. 2006 The residence time of river water in reservoirs. *Ecological Modelling* **191** (2), 260–274. https://doi.org/10.1016/j.ecolmodel.2005.04.030.

Samal, N. R., Mazumdar, A., Jöhnk, K. D. & Peeters, F. 2009 Assessment of ecosystem health of tropical shallow waterbodies in eastern India using turbulence model. *Aquatic Ecosystem Health & Management* **12** (2), 215–225. https://doi.org/10.1080/14634980902908589.

Scanlon, T., Moreau, J. & Stickland, M. 2020 *A Hydrodynamic Model of the West Coast of Scotland with Coupled Sea Lice Dispersion*. In: Breugem, W. A., Frederickx, L., Koutrouveli, T., Chu, K., Kulkarni, R. & Decrop, B. (eds.): Proceedings of the papers submitted to the 2020 TELEMAC-MASCARET User Conference October 2021. Antwerp: International Marine and Dredging Consultants (IMDC). S. 160–167. Available from: https://hdl.handle.net/20.500.11970/108307

Smolders, S., Maximova, T. & Vanlede, J. 2015 *Salinity in the 3D TELEMAC Model Scaldis (the Scheldt Estuary): Tracer Diffusion, Dispersion and Numerical Diffusion*. Available from: https://www.researchgate.net/publication/282973633

TELEMAC-3D. 2020 *TELEMAC-3D User Manual Version v8p2*.

Tessema, N., Kebede, A. & Yadeta, D. 2021 Modelling the effects of climate change on streamflow using climate and hydrological models: The case of the Kesem sub-basin of the Awash River basin. *Ethiopia. International Journal of River Basin Management* **19** (4), 469–480. https://doi.org/10.1080/15715124.2020.1755301.

Vouk, I., Murphy, E., Church, I., Pilechi, A. & Cornett, A. 2019 Three-dimensional modelling of hydrodynamics and thermosaline circulation in the Saint John River Estuary, Canada. In: *38th IAHR World Congress - 'Water: Connecting the World'*. Vol. 38, pp. 1866–1875. https://doi.org/10.3850/38wc092019-0895.

WAQTEL. 2021 *Technical Manual Version v8p3*. Available from: http://wiki.opentelemac.org/doku.php?id=documentation_v8p4r0. (accessed June 2023).

Williams, G. P. 1963 Heat transfer coefficients for natural water surfaces. *International Association of Scientific Hydrology* **62**, 203–212.

Yang, P., Fong, D. A., Lo, E. Y. M. & Monismith, S. G. 2019 Circulation patterns in a shallow tropical reservoir: Observations and modeling. *Journal of Hydro-Environment Research* **27**, 75–86. https://doi.org/10.1016/J.JHER.2019.09.002.

Ziaie, R., Mohammadnezhad, B., Taheriyoun, M., Karimi, A. & Amiri, S. 2019 Evaluation of thermal stratification and eutrophication in Zayandeh Roud Dam reservoir using two-dimensional CE-QUAL-W2 model. *Journal of Environmental Engineering* **145** (6). https://doi.org/10.1061/(ASCE)EE.1943-7870.0001529.

First received 18 September 2023; accepted in revised form 18 November 2023. Available online 2 January 2024